Highly siderophile element composition of the Earth's primitive upper mantle: Constraints from new data on peridotite massifs and xenoliths

H. Becker [a,b,*], M.F. Horan [c], R.J. Walker [a], S. Gao [d], J.-P. Lorand [e], R.L. Rudnick [a]

[a] *Department of Geology, University of Maryland, College Park, MD 20742, USA*
[b] *Institut für Geologische Wissenschaften, FR Geochemie, Freie Universität Berlin, Malteserstrasse 74-100, Haus B, D-12249 Berlin, Germany*
[c] *Department of Terrestrial Magnetism, Carnegie Institution of Washington, 5241 Broad Branch Road, NW Washington, DC 20015, USA*
[d] *Key Laboratory of Continental Dynamics, Department of Geology, Northwest University, Xi'an 710069, China*
[e] *Mineralogie-Petrologie, MNHN no 201 and CNRS UMR 7160, National Museum of Natural History, 61 Rue Buffon, 75005 Paris, France*

Abstract

Osmium, Ru, Ir, Pt, Pd and Re abundances and $^{187}Os/^{188}Os$ data on peridotites were determined using improved analytical techniques in order to precisely constrain the highly siderophile element (HSE) composition of fertile lherzolites and to provide an updated estimate of HSE composition of the primitive upper mantle (PUM). The new data are used to better constrain the origin of the HSE excess in Earth's mantle. Samples include lherzolite and harzburgite xenoliths from Archean and post-Archean continental lithosphere, peridotites from ultramafic massifs, ophiolites and other samples of oceanic mantle such as abyssal peridotites. Osmium, Ru and Ir abundances in the peridotite data set do not correlate with moderately incompatible melt extraction indicators such as Al_2O_3. Os/Ir is chondritic in most samples, while Ru/Ir, with few exceptions, is ca. 30% higher than in chondrites. Both ratios are constant over a wide range of Al_2O_3 contents, but show stronger scatter in depleted harzburgites. Platinum, Pd and Re abundances, their ratios with Ir, Os and Ru, and the $^{187}Os/^{188}Os$ ratio (a proxy for Re/Os) show positive correlations with Al_2O_3, indicating incompatible behavior of Pt, Pd and Re during mantle melting. The empirical sequence of peridotite-melt partition coefficients of Re, Pd and Pt as derived from peridotites ($D_{Re}^{s/l} < D_{Pd}^{s/l} < D_{Pt}^{s/l} < 1$) is consistent with previous data on natural samples. Some harzburgites and depleted lherzolites have been affected by secondary igneous processes such as silicate melt percolation, as indicated by U-shaped patterns of incompatible HSE, high $^{187}Os/^{188}Os$, and scatter off the correlations defined by incompatible HSE and Al_2O_3. The bulk rock HSE content, chondritic Os/Ir, and chondritic to subchondritic Pt/Ir, Re/Os, Pt/Re and Re/Pd of many lherzolites of the present study are consistent with depletion by melting, and possibly solid state mixing processes in the convecting mantle, involving recycled oceanic lithosphere. Based on fertile lherzolite compositions, we infer that PUM is characterized by a mean Ir abundance of 3.5 ± 0.4 ng/g (or $0.0080 \pm 0.0009*CI$ chondrites), chondritic ratios involving Os, Ir, Pt and Re (Os/Ir$_{PUM}$ of 1.12 ± 0.09, Pt/Ir$_{PUM} = 2.21 \pm 0.21$, Re/Os$_{PUM} = 0.090 \pm 0.002$) and suprachondritic ratios involving Ru and Pd (Ru/Ir$_{PUM} = 2.03 \pm 0.12$, Pd/Ir$_{PUM} = 2.06 \pm 0.31$, uncertainties 1σ). The combination of chondritic and modestly suprachondritic HSE ratios of PUM cannot be explained by any single planetary fractionation process. Comparison with HSE patterns of chondrites shows that no known chondrite group perfectly matches the PUM composition. Similar HSE patterns, however, were found in Apollo 17 impact melt rocks from the Serenitatis impact basin [Norman M.D., Bennett V.C., Ryder G., 2002. Targeting the impactors: siderophile element signatures of lunar impact melts from Serenitatis. Earth Planet. Sci. Lett., 217–228.], which represent mixtures of chondritic material, and a component that may be either of meteoritic or indigenous origin. The similarities between the HSE composition of PUM and the bulk composition of lunar breccias establish a connection between the late accretion history of the lunar surface and the HSE composition of the Earth's mantle. Although late accretion following core formation is still the most viable explanation for the HSE abundances in the Earth's mantle, the "late veneer" hypothesis may require some modification in light of the unique PUM composition.

---

* Corresponding author. Fax: +49 30 83870170.
  E-mail addresses: hbecker@zedat.fu-berlin.de (H. Becker), horan@dtm.ciw.edu (M.F. Horan), rjwalker@geol.umd.edu (R.J. Walker), jplorand@mnhn.fr (J.-P. Lorand), rudnick@geol.umd.edu (R.L. Rudnick).

1. Introduction

Core formation likely stripped the silicate Earth of the highly siderophile elements (HSE) Re, Os, Ir, Ru, Pt, Rh, Pd and Au, but the extent to which this might have occurred remains controversial, due, in part to uncertainties in the pressure- and temperature-dependence of HSE metal-silicate partition coefficients (Righter et al., 2000). Some workers have proposed that HSE might become much less siderophile at high pressures and temperatures (Murthy, 1991; Righter and Drake, 1997), while other work suggests that metal-silicate distribution coefficients for at least some of these elements are $>10^6$ at both low and high pressures (Holzheid et al., 2000; Ertel et al., 2001). In spite of this inferred nearly quantitative removal, HSE in the upper mantle are only approximately 150 times less abundant than in chondritic meteorites, and occur in broadly chondritic proportions. A variety of models have been proposed to explain these observations. Many authors have argued for a late influx or "veneer" of large planetesimals after formation of the Earth's core and the Moon (Chou, 1978; Jagoutz et al., 1979; Morgan, 1986; O'Neill, 1991; Drake, 2000; Schmidt et al., 2000; Meisel et al., 2001; Morgan et al., 2001; Schmidt, 2004). The late influx may have added up to 0.4% of the total mass of the Earth, depending on accretion rates and on HSE abundances in the Earth's lower mantle (Morgan et al., 2001). Aside from pressure- and temperature-dependent variation of metal-silicate partition coefficients (Murthy, 1991; Righter and Drake, 1997), alternative models proposed to explain the HSE composition of the mantle include inefficient core formation (Jones and Drake, 1986), addition of material from the outer core (Snow and Schmidt, 1998) and some specific homogeneous accretion scenarios (Kramers, 1998). The most compelling evidence in favor of the late influx hypothesis are the observed, broadly chondritic abundance ratios and isotopic ratios of HSE. Other hypotheses may have difficulty in explaining chondritic ratios, particularly in the light of the divergent chemical behavior of the HSE during planetary partitioning processes (Righter et al., 2000; Walker, 2000).

If the HSE in the upper mantle were added as part of a late influx, then their isotopic and relative abundance characteristics may shed light on the provenance of the materials added. Critical to this effort is characterization of the HSE composition of the primitive upper mantle (PUM, Meisel et al., 2001). PUM represents the composition of a hypothetical upper mantle reservoir that has never undergone depletion in basaltic components by melting processes. PUM is used instead of primitive mantle or bulk silicate Earth, because samples on which these estimates are based invariably originate from the upper mantle and no direct measurements of the HSE composition of lower mantle materials exist. As such, true PUM probably does not exist anywhere within the Earth. This is supported by radiogenic isotopes of lithophile incompatible elements such as ^{143}Nd and ^{87}Sr, indicating prior melt extraction, recycling of oceanic crust and mixing with depleted mantle for most basalts and peridotites derived from the upper mantle (Zindler and Hart, 1986; Hofmann, 1997). Thus, instead of direct measurements, viable estimates of the composition of PUM must be made via extrapolations from peridotites that show a composition close to PUM.

For moderately incompatible or compatible elements, such as the HSE, mantle materials with histories of only limited melt extraction may approximate the characteristics of PUM, and large extrapolations may not be required. Morgan (1986) used correlations between lithophile indicators of melt extraction and HSE abundances of upper mantle xenoliths to constrain the partitioning behavior of the HSE during mantle melting and to estimate the concentrations and relative abundances of some HSE in the PUM. Similarly, Meisel et al. (2001) applied linear correlations between ^{187}Os/^{188}Os (reflecting long-term Re/Os of the samples) and lithophile element indicators of melt extraction for worldwide suites of peridotite xenoliths from subcontinental lithospheric mantle, and orogenic peridotites, to obtain a minimum ^{187}Os/^{188}Os of 0.1296 ± 8 for modern PUM. This value is similar to measured ^{187}Os/^{188}Os in some ordinary and enstatite chondrites, but different from values in carbonaceous chondrites (Chen et al., 1998; Walker et al., 2002). Abundances of other HSE in PUM have been less well resolved, because of relatively large scatter of previous data on terrestrial peridotites and chondrites. New Ir, Ru, Pt and Pd data on chondrites obtained by isotope dilution and Carius tube digestion in reverse aqua regia (Horan et al., 2003) show considerably reduced scatter compared to earlier neutron activation data, and provide improved resolution of some differences in the HSE composition of chondrite groups. The data of Horan et al. (2003) may serve as a much improved basis for the comparison with terrestrial material.

In the past, two major issues have been associated with the determination and interpretation of HSE abundances in peridotites and other terrestrial samples. First, recent experimental studies have shown that it is difficult to completely digest large samples (>gram size) of ultramafic rocks for the analysis of HSE abundances (Shirey and Walker, 1995; Gros et al., 2002; Meisel et al., 2003a,b; Meisel and Moser, 2004; Puchtel et al., 2004; Puchtel and Humayun, 2005). Complete digestion is a prerequisite for the most precise concentration measurements involving solution chemistry and external or internal calibration techniques such as standard addition and isotope dilution. In particular, refractory phases such as spinel and platinum group element (PGE) alloys are notoriously difficult to

dissolve. This may result in poor yields and incomplete sample-spike equilibration. Meisel et al. (2003a,b) obtained encouraging results for the reproducibility and accuracy of HSE abundances in ultramafic reference materials using isotope dilution and digestion in reverse *aqua regia* in a high pressure asher at 300–320 °C. These studies also suggest that digestion techniques based on open beaker attack in HF–HNO$_3$, NiS fire assay or reverse *aqua regia* in Carius tubes at 220–240 °C may not always result in complete digestion. Other recent work on ultramafic reference materials using isotope dilution coupled with reverse aqua regia digestion in Carius tubes at lower temperatures has resulted in precisions of HSE abundances that are comparable to the high-pressure asher data (Pearson et al., 2004; Puchtel et al., 2004). Digestion issues may have affected reproducibility and accuracy of some previous HSE analyses of peridotites, particularly those where digestion was performed using the NiS fire assay technique (Morgan et al., 2001). Improved digestion techniques may lead to better analytical resolution, which in turn may provide new constraints on the origin of the HSE in the Earth's upper mantle.

The second issue concerns the possibility of addition or mobilization of HSE as a result of chemical reaction of melt or fluid percolating through the mantle ("metasomatism"). The process of chemical reaction of mafic melt with lithospheric mantle has been studied extensively using lithophile major and trace elements and radiogenic and stable isotopes (Bodinier and Godard, 2003; Pearson et al., 2003). Such secondary processes have been proposed to explain suprachondritic Pd/Ir in fertile peridotites (Pattou et al., 1996; Lorand et al., 1999; Rehkämper et al., 1999a; Pearson et al., 2004), however, analytical problems also may have contributed to enhanced Pd/Ir. Systematic studies of Os isotopic compositions and HSE abundances in spatially controlled samples from peridotite massifs show macroscopic and geochemical evidence for different styles of melt percolation (Becker et al., 2001b; Büchl et al., 2002). These studies indicate that dissolution and precipitation processes in zones of focused melt flow (high melt/rock ratios) may lead to substantial HSE redistribution and fractionation of HSE ratios (e.g., Os/Ir and Pt/Ir) and increased ^{187}Os/^{188}Os in reacted mantle rocks. More recent work has revealed that a substantial number of peridotite xenoliths yield Ir-group PGE (Os, Ir and Ru) and sometimes S abundances that are low compared with data from peridotite massifs (see data compilation and discussion in Pearson et al., 2004; Reisberg et al., 2005). In situ PGE data on sulfides and suprachondritic ^{187}Os/^{188}Os in some of these samples have implicated melt percolation in the mantle as the culprit (Alard et al., 2000, 2002; Lorand and Alard, 2001; Schmidt and Snow, 2002). One major conclusion emerging from these studies has been that such strongly modified mantle rocks are not suitable for deriving HSE abundances and ratios in the upper mantle. It also appears that peridotite xenoliths may yield a biased picture of the HSE distribution in the lithospheric mantle (Pearson et al., 2004; Reisberg et al., 2005).

In the present study, samples from peridotite massifs and xenoliths from various tectonic settings were analyzed for Os, Ir, Ru, Pt, Pd and Re abundances and their Os isotopic composition. Improved analytical techniques were employed in order to increase precision and accuracy of the concentration data. Emphasis has been placed on selecting fertile and moderately depleted peridotites, and to avoid mantle rocks that show evidence for strong modification by melt percolation. The objective of this study is to precisely and accurately characterize the HSE characteristics of peridotites, with particular focus on lherzolites, and provide an updated estimate of PUM. Major questions we address are: (1) Is there a dominant signature of HSE in fertile lherzolites? (2) Can this signature be tied to precursor materials that experienced particular nebular or other early solar system processes or does it reflect a global igneous process on Earth? (3) Does the upper mantle of the Earth exhibit heterogeneities in the relative abundances of HSE that cannot be attributed to indigenous processes? The new data will be discussed in the context of previous results and constraints for the origin of the HSE in the Earth's mantle and data for chondrites and lunar impact melt breccias.

2. Sample selection

Samples analyzed in the present study include lherzolite and harzburgite xenoliths and samples from peridotite massifs that display a range of fertility and occur in different tectonic settings. Most of these samples have been well-studied by previous investigators. Details are summarized in Table 1. There is a consensus that the primitive mantle has a major element composition resembling fertile lherzolite (Jagoutz et al., 1979; Ringwood, 1979; Sun, 1982; Palme and Nickel, 1985; Hart and Zindler, 1986; McDonough and Sun, 1995). For this reason, post-Archean continental peridotites are the main focus of the present study, because in these environments, fertile peridotites are more common than in Archean lithospheric mantle. For the same reasons, we have analyzed only relatively few oceanic peridotites such as abyssal peridotites, and peridotites related to ophiolites, because these materials may be biased towards highly depleted compositions that are residues from the top of the melting column beneath ocean ridges. Also included in the diagrams and discussion of the present study were some of the harzburgite and lherzolite data from the Troodos ophiolite published by Büchl et al. (2002), because these data were obtained by isotope dilution and digestion in a high-pressure asher at 300 °C, similar to this study.

It has been suggested that melt percolation at high melt/rock ratios may affect PGE and Re abundances and the ^{187}Os/^{188}Os of peridotites (Rehkämper et al., 1999a; Becker et al., 2001a,b; Büchl et al., 2002). Although details of these processes, and the extent to which that happens in various tectonic settings and lithologies (lherzolite vs. harzburgite) are not yet fully understood, rocks that were obviously

Table 1
Details on rock types and locales

Locale	Rock types	References
Post-Archean continental lithospheric mantle		
Lherz, Eastern Pyrenees	Lh, Hz (m) s	(Bodinier et al., 1988; Reisberg and Lorand, 1995;
Turon de Tecouere, Western Pyrenees, France	Lh (m) s	Pattou et al., 1996; Lorand et al., 1999)
Northern and central Lanzo massif, Italian Alps	Lh (m) s	(Bodinier, 1988; Bodinier et al., 1991; Lorand et al., 1993, 2000)
Ronda, Betic Cordillera, Spain	Lh (m) s	(Reisberg et al., 1991; Reisberg and Lorand, 1995; Lorand et al., 2000)
Hannuoba, China	Lh, Hz (x)	(Gao et al., 2002; Rudnick et al., 2004)
Lower Austria	Lh, Hz (m) s	(Becker, 1996; Becker et al., 2001a,b)
Ashaway lamprophyre dike, R. I., USA	Lh, Hz (x)	(Minarik, pers. comm.)
Kilbourne Hole, N.M., USA	Lh (x)	(Morgan, 1986; Meisel et al., 2001)
San Carlos, AZ., USA	Hz (x)	(Morgan, 1986; Meisel et al., 2001)
San Quintin, Mexico	Lh (x)	(Morgan, 1986; Meisel et al., 2001)
Mt. Quincan, Queensland, Australia	Lh (x)	(Morgan, 1986; Meisel et al., 2001)
Archean continental lithospheric mantle		
Labait, Tanzania	Lh, Hz (x)	(Chesley et al., 1999; Lee and Rudnick, 1999)
Matsoku, Lesotho	Lh, Hz (x)	(Morgan, 1986; Meisel et al., 2001)
Phanerozoic oceanic peridotites (ophiolites and abyssal peridotites)		
Luobusha Ophiolite, Tibet, China	Lh (m)	
Totalp Peridotite, Swiss Alps	Lh (m) s	(Peters and Stettler, 1987), Becker (unpublished data)
Fernando de Noronha, Brazil	Lh (x)	Sichel (pers. comm.)
St. Paul Fracture Zone, Atlantic Ocean	Hz, s	Sichel (pers. comm.)
Kane Fracture Zone, Site 920, Atlantic Ocean	Hz, s	(Brandon et al., 2000)

Lh, lherzolithe; Hz, harzburgite; m, peridotite massif; x, xenoliths; s, serpentinized.

modified by melt percolation, such as replacive dunites, were excluded from consideration. Evidence will be presented that the HSE composition of some of the massif and xenolith samples examined may have been affected by melt percolation. Apart from obtaining worldwide coverage, another criteria for selection of particular sample suites has been previous data showing well defined correlations of Re, $^{187}Os/^{188}Os$ or sulfur abundances with lithophile melt extraction indices such as Al_2O_3 (Pyrenees, Hannuoba, SW-USA). Such correlations are indicative of a relatively simple history and suggest that these elements were little affected by weathering and serpentinization. Samples from the Pyrenees, Lanzo and Ronda were previously analyzed for PGE abundances using NiS fire-assay digestion and ICPMS or neutron activation techniques (NAA). A brief comparison of some of these data with the new results is given in the Appendix A.

3. Analytical techniques

Abundances of Os, Ir, Ru, Pt, Pd and Re were determined by isotope dilution using a mixed ^{185}Re–^{190}Os spike and a mixed ^{191}Ir–^{104}Ru–^{198}Pt–^{110}Pd spike of roughly chondritic proportions. These mixed spikes were the same spikes as those used for the analysis of chondrites by Horan et al. (2003) and Walker et al. (2002), hence, any analytical bias associated with spike calibrations will be the same for chondrites and peridotites. Some peridotites were analyzed using a new mixed ^{191}Ir–^{99}Ru–^{194}Pt–^{105}Pd spike that was calibrated using the same standards as for the mixed ^{191}Ir–^{104}Ru–^{198}Pt-^{110}Pd spike.

3.1. Digestion

In order to facilitate complete digestion, we have employed a modified closed-system digestion technique using 9 ml reverse *aqua regia* and quartz glass Carius tubes at 345 °C. The amount of sample was typically 2–3 g, however, in some cases (UM17, UM19) only 0.3–0.5 g of material was available. After adding samples and spikes the tubes were sealed and predigested at 220 °C overnight. After cooling and subsequent agitation in an ultrasonic bath, the tubes were inserted into a steel pressure vessel containing 20 g dry ice. The CO_2 pressure that builds up inside the pressure vessel upon warming supports the internal pressure in the Carius tube at 345 °C. Inspection of sealed tubes under the binocular microscope revealed that in most cases, and almost always in the case of fresh peridotite samples, abundant spinel grains remained undigested after overnight digestion at 220 °C. In contrast, after two more days of high-temperature digestion at 345 °C, spinels were either completely dissolved, or oxidized and replaced by tiny brownish "rust balls". Complete digestion of spinel is important because it commonly hosts inclusions of PGE alloys and sulfides. Another prerequisite for successful digestions is that rock powders are ground as finely as possible (<10 μm). A test showed that for a sample containing a fraction of coarser material complete digestion of spinels was not achieved even at high temperatures. It should also be noted that even at 345 °C, clinopyroxene appears undigested, and orthopyroxene may only be partially digested. Hence, it is important that powders are fine enough so that HSE-bearing sulfide and alloy inclusions are exposed to the

acid. The process of serpentinization may be helpful in pre-digesting peridotites. Heavily serpentinized samples show a larger proportion of their silicates converted to gel-like compounds than unaltered peridotites.

3.2. Chemical separation

Osmium was separated by solvent extraction from reverse *aqua regia* into CCl_4 and back extraction into HBr, followed by micro distillation (Becker et al., 2001a). After evaporation of most of the *aqua regia*, and dissolution of the residue in 10 ml of 0.8 M HNO_3 and 0.5 ml 30% H_2O_2, Re, Ru, Ir, Pt and Pd were separated from the matrix by anion exchange chromatography using 2 ml of pre-cleaned Biorad AG 1-X8 or Eichrom 1-X8 resin. After matrix elution in 15 ml 0.8 M HNO_3, Re + Ru, and Ir + Pt + Pd were successively collected as two separate fractions in 10 ml of 15 M HNO_3 each. The Re–Ru and Ir–Pt–Pd fractions were taken to near-dryness, and were repeatedly fluxed with *aqua regia*, HF, and HNO_3 in order to remove silica, and organics. Finally, the two fractions were dissolved in 3–4 ml 2% HNO_3.

3.3. Mass spectrometry

Osmium isotopic ratios were measured on Faraday cups by negative thermal ionization mass spectrometry using a Sector 54 multi collector instrument (Becker et al., 2001a). A few samples were run on the UMD NBS 12-in. radius single collector instrument using either a Faraday cup or an electron multiplier in the pulse counting mode. External precisions for Faraday runs are 0.1% (2σ) or better, and 0.3% (2σ) for electron multiplier runs (Samples L215, UM17, AP3). Precisions are based on 2σ precisions obtained on multiple runs of the UMD Os standard over periods of several months.

The Re–Ru and Ir–Pt–Pd cuts were run separately on the UMD Thermo Electron Element 2 magnetic sector ICPMS in the E-scan mode. Signals were detected using an electron multiplier in the pulse counting mode. To increase sensitivity and reduce oxide formation, the solutions were aspirated into the plasma with an Aridus desolvating nebulizer at flow rates of 30–150 µl/minute. An analysis typically consisted of 400 scans over the sequence of masses 99, 101, 102, 104 (Ru), 105, 106, 108, 110 (Pd), 111 (Cd), 185, 187 (Re), 189 (Os), 191, 193 (Ir), 194, 195, 196, 198 (Pt), and 199 (Hg). The dwell time on each mass peak was 40 ms. Cadmium, Os and Hg masses were scanned to monitor possible isobaric interferences on [110]Pd, [187]Re and [198]Pt. For samples analyzed using the [191]Ir–[104]Ru–[198]Pt–[110]Pd spike such interferences were small (Typically < 1% interference from [110]Cd on [110]Pd) or insignificant. Interferences from [104]Pd on [104]Ru were minor in a few cases (<7%), but mostly insignificant. Interferences were not an issue for those samples for which the [191]Ir–[99]Ru–[194]Pt–[105]Pd spike was used.

A mixed Re–Ir–Ru–Pt–Pd standard with roughly chondritic abundance ratios and 600 pg/g Ir was analyzed at the beginning, and sometimes at the end of each analysis session to monitor mass discrimination and possible drift of the instrument. Isotopic ratios of samples were corrected for mass fractionation using an exponential mass fractionation law and ratios measured for the standard. Washout times in-between samples were between 5 and 7 min. On-peak zeroes for the 2% nitric acid solution were taken after every 4 samples to monitor potential memory effects. Total chemistry blanks run in the course of this study ($n = 5$) were 0.8–1.8 pg for Re, 0.7–2.7 pg for Os, 1–70 pg for Ir, 3–199 pg for Ru, 3–26 pg for Pt and 9–376 pg for Pd (Table 2). Relatively high blanks for Pd were noted while using the Biorad resin, hence, the switch to Eichrom 1-X8. With the exception of Pd and Re in highly depleted harzburgites (71325, LB14, KAT-1, UM10), blank corrections were negligible or minor (<2%).

In-run precisions of isotopic ratios measured on the Element 2 were between 0.2 and 1% $(2\sigma_m)$. Accuracy and reproducibility of concentrations were tested by multiple analysis of reference material UB–N, a serpentinized lherzolite (Table 2). This material has been analyzed many times for PGE and Re using isotope dilution and digestion in a high-pressure asher at 300 °C or Na_2O_2–NaOH fusion (Meisel et al., 2003a,b; Meisel and Moser, 2004). Reproducibility of UB–N data from the present study ranges from 1.9% RSD for Re to 5.0% RSD for Ru, while HSE ratios are reproducible to 3–7% (RSD). This variability compares well with other data obtained by state-of-the-art techniques and largely reflects sample heterogeneity (Meisel et al., 2003a,b; Meisel and Moser, 2004). With the exception of Os, the mean of our four analyses of UB–N lies within the uncertainty of the literature data (Table 2, Fig. 1). The mean Os abundance of UB–N in this study (3.51 ng/g) is 5.4% lower than that in Meisel and Moser (2004), while Re abundances agree within 1%. In principle, these discrepancies could reflect errors in spike calibrations, incomplete digestion of our UB–N aliquots or heterogeneities in the UB–N sample powder. Errors in spike calibrations of that magnitude appear unlikely. Our mixed Re–Os spike represents a dilution of the concentrated mixed spike used by Smoliar et al. (1996) for determination of the [187]Re decay constant based on an iron meteorite isochron. The decay constant determined by Smoliar et al. (1996) agrees with an independent determination at the 1% level (Shen et al., 1996). Thus, given the close agreement of our Re concentrations for UB–N with the literature data, Os concentrations should be as accurate as those for Re, provided, complete digestion was achieved. Because our Ir and Ru data for UB–N show good agreement with the literature data, and our digestions were performed at higher temperatures than other comparable studies, we consider it unlikely that digestion issues are involved. Osmium concentrations of UB–N determined in previous work, using the most reliable digestion techniques (alkaline fusion and high-P asher at 300 °C), show some variability between

Table 2
Results for total chemistry blanks, reference material UB–N and the CV3 chondrite Allende

Sample	T (°C)	Os	Ir	Ru	Pt	Pd	Re	$^{187}Re/^{188}Os$	$^{187}Os/^{188}Os$
				Concentrations in ng (blanks) or ng/g					
Total chemistry blanks									
[a]	320	0.0007	0.019	0.003	0.008	0.376	0.0018		
[a]	345	0.0023	0.070	0.020	0.026	0.141	0.0018		
[b]	345	0.0013	0.001	0.085	0.003	0.009	0.0018		
[b]	345	0.0027	[c]	[c]	0.006	0.070	0.0018		
[b]	345	0.0025	0.005	0.199	0.015	0.313	0.0008		
Reference material UB–N (ANRT) distributed by CRPG–CNRS (Nancy, France)									
UB–N 1	320	3.59	3.42	6.92	7.03	5.99	0.200	0.269	0.12780
UB–N 2	345	3.51	3.30	6.57	7.29	6.06	0.203	0.279	0.12743
UB–N 3	345	3.60	3.14	6.39	6.74	5.47	0.206	0.276	0.12714
UB–N 4	345	3.33	3.17	6.14	6.95	5.90	0.209	0.302	0.12712
Mean		**3.51**	**3.26**	**6.51**	**7.00**	**5.85**	**0.205**	**0.282**	**0.12737**
% RSD		3.5	3.9	5.0	3.3	4.5	1.9	5.2	0.2
UB–N Lit.[d]	300	**3.71**	**3.38**	**6.30**	**7.42**	**6.11**	**0.206**		
% RSD		7.1	6.4	4.6	4.0	2.9	2.4		
UB–N Lit.[e]		**3.64**	**3.52**	**7.24**	**7.48**	**6.10**	**0.197**		
% RSD		12	11	11	4	4	13		
Allende[f]	345	763	700	1140	1379	786	61.2	0.3860	0.12638

T, digestion temperature; RSD, relative standard deviation; Bold represents mean values.
[a] Anion exchange resin Biorad AG 1-X8.
[b] Anion exchange resin Eichrom 1-X8.
[c] Signal intensity too low.
[d] High-pressure asher data of Meisel et al. (2003a) and Meisel and Moser (2004).
[e] Carius tube data at 240 or 270 °C, Puchtel and Humayun (2005).
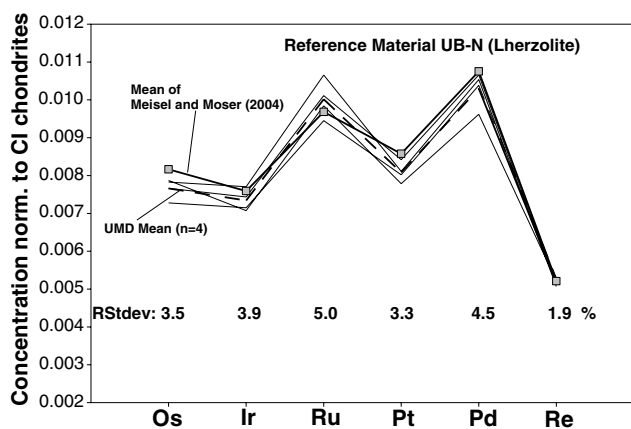[f] 0.09 g of Smithsonian Allende standard powder.

Fig. 1. Os, Ru, Ir, Pt, Pd and Re concentration data for the reference material UB–N (serpentinized lherzolite), normalized to the mean of CI chondrite data of Horan et al. (2003). Note the linear scale. Shown are individual analyses, their mean value (UMD Mean, dashed line), relative standard deviation, and a comparison with mean concentrations of HSE in UB–N (gray squares) from Meisel and Moser (2004).

3.31 and 4.41 ng/g Os (Meisel et al., 2003a,b). The concentration range found in the present study lies within that range. We also note that the mean Os concentration for UB–N obtained by Puchtel and Humayun (2005) lies between our average and that of Meisel and Moser (2004). Hence, heterogeneity of the UB–N sample powder may be at present the most viable explanation for differences in mean Os abundances of UB–N between different studies.

4. Results

A comparison of the new data with results obtained by other techniques on the same samples is given in the Appendix A. In Table 3, results from previous Re–Os studies on the same samples, using low-temperature digestion (220–230 °C) are included. Here, we only highlight the differences that have a major impact on data interpretation. Foremost, the new Ir and Ru abundances for the Pyrenean peridotites are systematically higher (up to 50% and more in some cases) than previous concentration data obtained on the same samples by NiS fire assay digestion and ICP-MS or NAA techniques (Pattou et al., 1996; Snow and Schmidt, 1998; Lorand et al., 1999). The high Pt and Pd abundances for peridotites from Lanzo reported by Lorand et al. (1993), could not be confirmed by the new and previous data (Lorand et al., 2000), which are comparable to Pt and Pd abundances in fertile and depleted lherzolites elsewhere. Due to the improved digestion technique and the use of isotope dilution for concentration determinations, the scatter of the data was considerably reduced (see Appendix A).

As with previously published peridotite data sets (see Pearson et al., 2004; for a compilation), concentrations of the Ir-group PGE Ir, Os and Ru correlate with each other (not shown). The overall peridotite data set of Ir-group PGE do not correlate with moderately incompatible HSE (e.g., Pd and Re) and lithophile melt extraction indicators such as Al_2O_3, however, larger data sets from individual locales (Pyrenees, Hannuoba) show

Table 3
PGE, Re, ^{187}Os/^{188}Os, Al$_2$O$_3$ and S data for peridotites

Sample	Rock	T	Os	Ir	Ru	Pt	Pd	Re	^{187}Re/^{188}Os	^{187}Os/^{188}Os	Al$_2$O$_3$[a] (wt%)	S[a] (μg/g)
					Concentrations in ng/g							
Continental peridotites												
Lherz (Eastern Pyrenees, France)												
71-107	L	HT	5.58	4.90	8.82	5.91	3.67	0.090	0.0777	0.11570	1.90	158
71-322	H	HT	4.03	4.76	9.08	7.06	3.60	0.046	0.0544	0.12325	1.53	56
71-325	H	HT	4.98	4.15	8.79	4.40	0.59	0.069	0.0671	0.11536	0.62	5
86-V2	L	HT	5.85	3.02	6.18	5.77	4.97	0.247	0.203	0.12773	3.58	250
82-4	H	HT	4.72	4.10	8.00	4.86	2.61	0.074	0.0755	0.11410	1.14	
Turon de Técouère (Western Pyrenees, France)												
TUR7	L	HT	4.03	3.59	7.22	7.20	6.54	0.341	0.408	0.12959	4.18	270
TUR11	L	HT	4.25	3.90	7.71	7.94	6.49	0.302	0.342	0.12590	3.36	190
TUR14	L	HT	3.66	3.26	6.82	6.90	6.35	0.345	0.454	0.12852	3.95	240
TUR16	L	HT	4.93	4.38	8.62	6.49	5.25	0.223	0.218	0.12009	2.2	140
TUR21	L	HT	4.90	4.23	8.34	7.98	6.81	0.409	0.401	0.12643	2.87	155
TUR23	L	HT	3.58	3.07	6.10	6.39	5.62	0.297	0.399	0.12883	3.7	220
TUR10	L	HT	3.87	3.46	7.28	6.93	6.65	0.283	0.352	0.12697	3.55	225
Lanzo (Italian Alps)												
L213	L	HT	3.25	2.89	5.66	5.78	4.47	0.261	0.387	0.12680	3.30	200
L216	L	HT	3.41	2.90	5.68	4.24	3.48	0.145	0.205	0.12020	2.29	100
L217	L	HT	3.90	3.59	7.28	5.83	5.38	0.279	0.344	0.12325	3.70	210
L92	L	HT	4.19	3.75	7.72	7.39	6.16	0.298	0.343	0.12550	3.20	142
L215	L	HT	3.67	2.53	6.27	7.41	6.41	0.243	0.318	0.12220	2.73	215
L66	L	HT	3.61	3.18	6.66	6.87	5.64	0.237	0.316	0.12619	3.14	168
Ronda (Betic Cordillera, Spain)												
RO144	L	HT	3.94	3.51	7.13	7.17	6.28	0.337	0.412	0.12779	3.39	240
RO-126	L	HT	3.91	3.49	6.79	6.54	5.35	0.311	0.383	0.12669	3	160
Lower Austria												
PW12	L	HT	3.83	3.34	7.36	5.45	3.52	0.127	0.160	0.11888	2.09	
		LT[b]	4.58					0.127	0.133	0.1194		
DW324-B	H	HT	3.99	3.52	7.05	5.19	3.13	0.052	0.0628	0.12009	1.39	
		LT[b]	4.19					0.055	0.0629	0.1202		
Ashaway (Rhode Island, US)												
Ash 01-2	L	HT	3.63	3.27	7.02	5.57	3.94	0.214	0.284	0.12034		
		LT	3.52					0.221	0.302	0.12012		
RB-5 #4	H	HT	2.98	2.66	5.54	3.99	2.80	0.086	0.139	0.11693		
		LT	2.86					0.082	0.137	0.11822		
Kilbourne Hole (New Mexico, US)												
UM-5	L	HT	2.60	2.72	5.52	5.15	3.48	0.142	0.263	0.12203	3.07	152
		LT[c]	2.56					0.220	0.414	0.12286		
UM-8	L	HT	3.10	3.40	6.34	4.87	2.75	0.064	0.099	0.12460	3.37	93
		LT[c]	3.07					0.216	0.339	0.12498		
San Carlos (Arizona, US)												
UM-10	H	HT	2.14	1.55	5.31	3.26	0.81	0.005	0.0122	0.12301	1.37	50
		LT[c]	1.84					0.012	0.031	0.12326		
San Quintin (Mexico)												
UM14	L	HT	2.60	2.83	5.62	2.41	1.21	0.050	0.0919	0.12197	2.86	55
		LT[c]	2.81					0.268	0.459	0.12288		
Labait (Tanzania)												
LB-4	H	HT	3.14	3.73	7.21	7.21	4.15	0.042	0.0647	0.12235	1.54	0.5
		LT[d]	2.60					0.175	0.320	0.1248		
LB14	H	HT	5.18	2.54	5.48	0.24	0.06	0.003	0.0028	0.10573	0.33	0.6
		LT[d]	4.85					0.058	0.0566	0.1081		
LB 45	L	HT	1.56	1.69	3.11	3.89	1.45	0.235	0.729	0.12784	3.89	0.3
		LT[d]	1.12					0.545	2.35	0.1329		
KAT-1	H	HT	4.94	4.14	6.87	1.60	0.37	0.003	0.0026	0.10807	0.65	0.03
		LT[d]	3.35					0.011	0.0150	0.1140		
Matsoku (Lesotho)												
UM17	L	HT	1.80	1.43	2.12	1.55	1.85	0.212	0.568	0.11532	2.45	
		LT[c]	2.67					0.194	0.350	0.11396		

Table 3 (*continued*)

Sample	Rock	T	Os	Ir	Ru	Pt	Pd	Re	^{187}Re/^{188}Os	^{187}Os/^{188}Os	Al$_2$O$_3$[a] (wt%)	S[a] (μg/g)
					Concentrations in ng/g							
UM19	H	HT	7.98	7.31	33.88	18.30	6.44	0.159	0.0960	0.11100	1.41	
		LT[c]	13.10					0.088	0.0320	0.11134		
Hannuoba (China)												
DMP56	L	HT	3.55	3.21	6.34	6.60	5.69	0.257	0.350	0.12748	3.49	260
		LT	3.70	3.52	6.96	7.11	6.32			0.12735		
		LT	3.62	3.42	6.90	7.18	7.43	0.233	0.303	0.12747		
		LT[e]	3.75					0.229	0.295	0.12769		
		LT[e]	3.64					0.232	0.308	0.12819		
DMP60	L	HT	4.00	3.59	7.24	7.31	6.21	0.303	0.365	0.12628	3.67	320
		HT	3.92	3.46	6.75	6.90	5.87	0.338	0.415	0.12626		
		LT	4.04	3.99	7.17	7.94	6.30	0.339	0.395	0.12657		
		LT	4.03	3.82	7.24	7.54	6.09	0.330	0.386	0.12621		
		250°		3.84	7.32	8.03	6.05	0.289				
		LT[e]	4.19					0.292	0.336	0.1267		
		LT[e]	4.10					0.293	0.345	0.1264		
DMP19	L	HT	4.13	4.34	8.54	8.53	6.66	0.181	0.211	0.11998	1.91	91
		LT	4.26	4.59	9.14	8.63	7.19	0.102		0.12026		
		LT[e]	4.35					0.108	0.119	0.1203		
DMP41	L	HT	2.91	3.00	5.82	5.50	4.25	0.172	0.285	0.12327	2.76	110
		LT	2.95	3.23	6.01	5.56	5.99	0.196	0.313	0.12346		
		LT[e]	2.92					0.158	0.260	0.1236		
DMP04	L	HT	3.76	3.56	7.41	6.62	4.96	0.211	0.271	0.12289	2.29	73
		LT	3.70	3.75	7.52	6.63	5.46	0.214	0.272	0.11678		
		LT	4.14	3.58	7.38	6.28	3.31	0.212	0.241	0.12298		
		LT[e]	3.95					0.198	0.241	0.1235		
		LT[e]	3.94					0.198	0.243	0.1231		
DMP58	L	HT	3.78	3.59	7.33	6.96	5.86	0.190	0.242	0.12539	3.16	230
		LT	3.95	3.75	7.26	7.08	5.75	0.193	0.230	0.12594		
		LT[e]	3.95					0.185	0.225	0.1259		
DMP25	H	LT	2.70	2.27	5.14	3.46		0.032	0.0558	0.11678	1.61	20
		LT[e]	3.26					0.032	0.0476	0.1166		
Mt. Quincan (Queensland, Australia)												
UM15	L	HT	1.37	2.09	3.95	4.71	2.35	0.156	0.548	0.12594	2.89	52
		LT[c]	1.45					0.377	1.26	0.12718		
Oceanic Peridotites												
Luobusha Ophiolite (Tibet, China)												
T97-93	L	HT	4.22	3.58	7.67	6.97	6.71	0.430	0.492	0.12350		
T97-101	L	HT	4.42	3.90	7.06	6.55	6.03	0.283	0.308	0.12230		
Totalp Serpentinite (Swiss Alps)												
TA15	L	HT	3.93	3.49	6.93	7.12	6.57	0.412	0.505	0.13103	4.34	
		LT	4.02					0.409	0.490	0.13110		
TA22A2	L	HT	3.41	3.25	6.09	4.66	4.78	0.171	0.242	0.12283	1.82	
		LT	2.88					0.170	0.285	0.12460		
St. Paul Fracture Zone Dredge (Atlantic Ocean)												
SP-8-02	H	LT	3.69	3.72	7.19	6.29	3.57	0.027	0.0355	0.12379	1.18	
Kane Fracture Zone Site 920 (Atlantic Ocean)												
AP-3	H	HT	3.90	2.83	6.58	6.18	4.49	1.660	2.05	0.12460	1.82	
		LT	4.21			6.45		0.425	0.486	0.12507		
AP-6	H	HT	4.54	3.48	5.05	7.88	7.64	0.474	0.504	0.12626	1.52	
		LT	4.03			8.34		0.431	0.515	0.12715		
Fernando de Noronha Xenolith (Atlantic Ocean)												
FN-X1	L	LT	3.83	3.67	7.24	6.49	5.03	0.511	0.643	0.1249		

L, lherzolite; H, harzburgite; T, digestion temperature; HT, high-temperature digestion (345 °C); LT, low-temperature digestion (220–240 °C).

[a] Literature (see text) and unpublished data.

[b] (Becker et al., 2001a,b).

[c] (Meisel et al., 2001).

[d] (Chesley et al., 1999).

[e] (Gao et al., 2002).

weak negative correlations with Al_2O_3 (Fig. 2). The Ir-group PGE show increasing variability of concentrations from lherzolitic to harzburgitic compositions such that very depleted samples may show both high and low concentrations for these elements (for instance Ir in Fig. 2 ranges between 1.6 and 7.3 ppb at low Al_2O_3). Fertile samples in contrast, show a much more narrow concentration range, typically 3–4 ppb Ir, with only few samples at low concentrations. Os/Ir and Ru/Ir (Figs. 3 and 4) are constant over a wide range of compositions
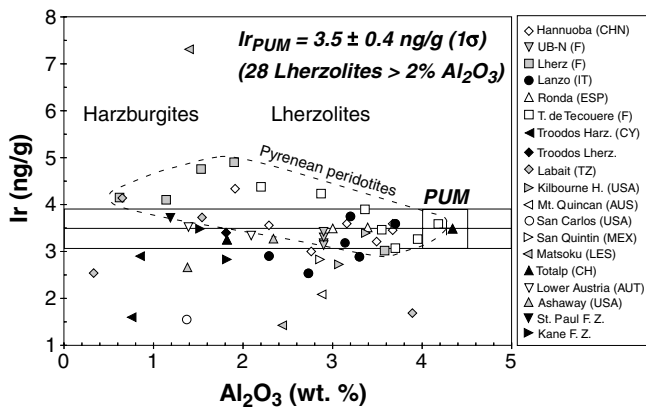
Fig. 2. Ir-Al_2O_3 diagram showing data for peridotites analyzed for this study and data from Büchl et al. (2002) for peridotites from the Troodos ophiolite. Only data obtained by high-temperature digestion in Carius tubes or high-pressure asher (>300 °C) are displayed. Here, and in Figs. 3–7, Al_2O_3 is used as a melt extraction indicator. Ir, Os, and Ru are compatible during mantle melting, and hence, show little systematic variation with Al_2O_3. A negative correlation for Pyrenean peridotites (squares) can be explained by mass loss through melt extraction and is outlined by the dashed line. For details regarding the estimated PUM values (small box) in this and the following diagrams, see Section 5.3 in the text.
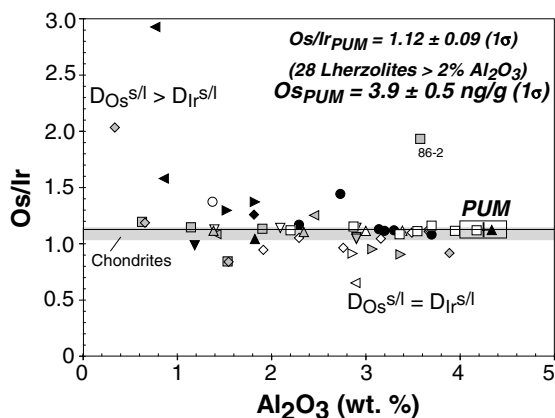
Fig. 3. Os/Ir–Al_2O_3 diagram. Except for a few outliers, Os/Ir is constant over a wide range of Al_2O_3 (suggesting similar peridotite-melt partition coefficients $D_{Os}^{s/l}$ and $D_{Ir}^{s/l}$) and appears to increase in highly depleted harzburgites, presumably because of an increase of $D_{Os}^{s/l}$ relative to $D_{Ir}^{s/l}$. Sample 86-V2 represents wallrock of a hornblendite dike and has anomalously high Os/Ir. The grey band indicates the range of Os/Ir in chondrites, which overlaps with the PUM estimate.
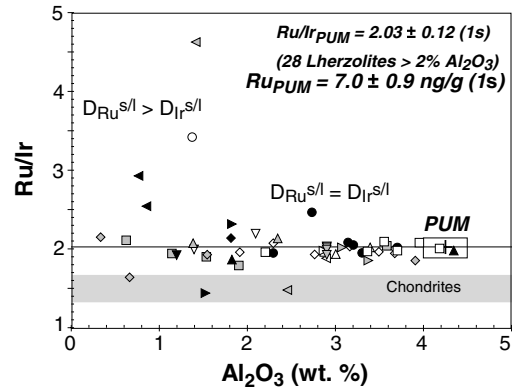
Fig. 4. Ru/Ir–Al_2O_3 diagram. Ru/Ir is constant over a wide range of Al_2O_3, and like Os/Ir, increases in highly depleted harzburgites, presumably because of an increase of $D_{Ru}^{s/l}$ relative to $D_{Ir}^{s/l}$. The grey band indicates the range of Ru/Ir in chondrites, which does not overlap with the PUM estimate (only two depleted peridotites have chondritic Ru/Ir). Ru/Ir$_{PUM}$ is suprachondritic.

(1–4.5 wt% Al_2O_3) but increase substantially in some harzburgites. Except for some highly Al-depleted samples, Os/Ir is chondritic or near chondritic in most peridotites. Some fertile lherzolites show slightly subchondritic Os/Ir and two lherzolites are suprachondritic. Except for harzburgites from the Kane fracture zone (AP-6), Tanzania (KAT-1), and a depleted lherzolite from Matsoku (UM-17), Ru/Ir is suprachondritic.

Concentrations of Pt, Pd and Re correlate positively with Al_2O_3 (not shown). The scatter in these correlations partly reflects sample heterogeneity and, decreases somewhat when ratios of these elements are plotted with Ir or Os in the denominator (Figs. 5–7), yet substantial scatter remains, particularly for Pt/Ir or Pt/Os (Figs. 6a and b). Re/Os (Fig. 5b) and Pd/Ir (Fig. 7a) correlate well with Al_2O_3, and, where data are available, with S (Fig. 7b). Some samples show deviations from these correlations, both to low and to high ratios for a given Al_2O_3 content. These variations sometimes reflect high concentrations of Re, Pt or Pd (for instance in samples AP-3, AP-6) and some of the Troodos samples from Büchl et al. (2002), anomalously low Ir concentrations (samples 86-2, L215), or low concentrations of Pt and Pd (samples UM8, UM14). A few samples show low abundances of all HSE, except Re (samples LB45, UM5, UM17), while unusual enrichment in HSE with variable fractionation of Pt, Pd and Re has been noted in one sample (UM19). The large variability in HSE abundances of Matsoku samples UM 17 and UM19 is consistent with similar observations made by Pearson et al. (2004). $^{187}Os/^{188}Os$ of different suites of peridotites correlate well with Al_2O_3 (Fig. 5a). Some depleted samples, however, plot off these correlations (e.g., 71322, LB4), possibly indicating that these samples were affected by addition of radiogenic Os. Among the different suites of peridotites, the Pyreneean samples show the best correlations.
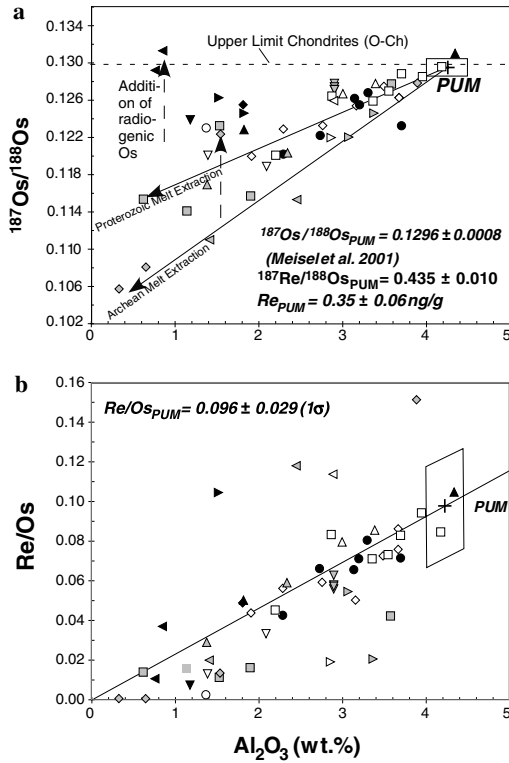
Fig. 5. (a) Measured $^{187}Os/^{188}Os$ vs. Al_2O_3 showing linear trends for some sample suites (Pyrenees, Hannuoba, Tanzania), reflecting long-term Re depletion resulting from variable melt extraction at different times in the past (Reisberg and Lorand, 1995; Meisel et al., 2001). Some samples show anomalous high $^{187}Os/^{188}Os$ at a given Al_2O_3 content, suggesting that they were affected by melt percolation at high melt/rock ratios (some data from Chesley et al., 1999; Brandon et al., 2000; Becker et al., 2001b; Büchl et al., 2002). The diagram also shows an upper limit for chondrites, represented by some ordinary chondrites (Walker et al., 2002). The PUM estimates for Re/Os and Re are based on the $^{187}Os/^{188}Os_{PUM}$ from Meisel et al. (2001). (b) Re/Os–Al_2O_3. The good correlation reflects incompatible behavior of Re and indicates limited Re mobility during alteration.

5. Discussion

5.1. Effects of partial melting

From previous studies of peridotites it has been known that Os, Ir and Ru behave compatibly up to moderately high degrees of melting of the Earth's mantle, whereas Au and Re are incompatible elements (Jagoutz et al., 1979; Morgan, 1986; Morgan et al., 2001; Pearson et al., 2004). The situation for Pt and Pd has been less clear. Both elements are depleted in harzburgites relative to lherzolites (Handler and Bennett, 1999; Lorand et al., 1999; Rehkämper et al., 1999a; Schmidt et al., 2000; Pearson et al., 2004), and show incompatible behavior in komatiites (Brügmann et al., 1987; Rehkämper et al., 1999b; Puchtel et al., 2004; Puchtel and Humayun, 2005), consistent with incompatible behavior at high degrees of melting. The absence of correlations of Pt and Pd with indices of melt extraction in previous studies of fertile and moderately depleted peridotites was inter-
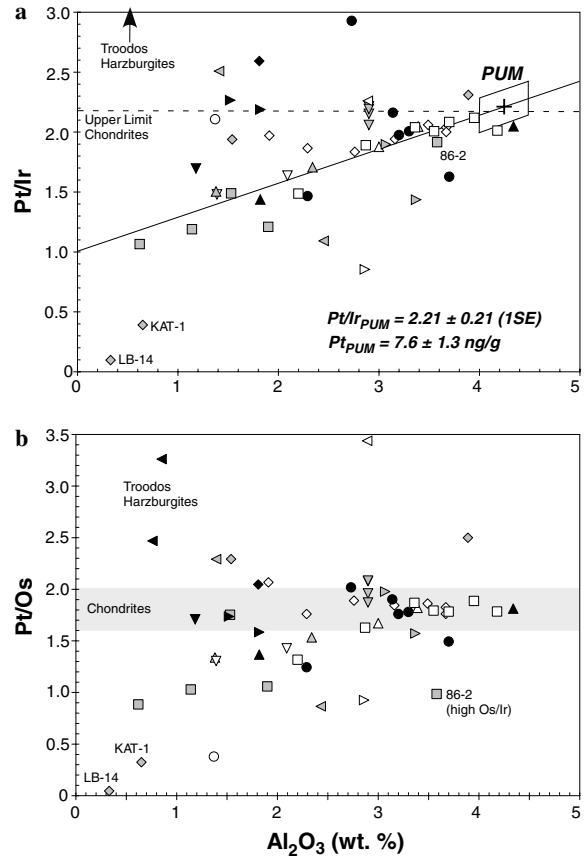
Fig. 6. (a) Pt/Ir–Al_2O_3 diagram. The slope of the correlation is shallower than the slope of Re/Os (Fig. 5b), Re/Ir (not shown) or Pd/Ir (Fig. 7) vs. Al_2O_3, suggesting that Pt is less incompatible than Re and Pd. In some depleted samples (some abyssal peridotites, samples from the Troodos ophiolite), Pt/Ir is enhanced or depleted and may have been affected by melt percolation or refertilization processes (see text). Pt/Ir$_{PUM}$ is chondritic. (b) Pt/Os–Al_2O_3 diagram. This diagram is shown because of its relevance for ^{190}Pt–^{186}Os systematics in the upper mantle (Walker et al., 1997, 2005; Brandon et al., 2000). Most samples are characterized by subchondritic or chondritic Pt/Os and are consistent with chondritic $^{186}Os/^{188}Os$ of upper mantle materials.

preted in terms of compatible behavior of these elements during low to moderate degrees of partial melting (Handler and Bennett, 1999; Lorand et al., 1999). In contrast, the data in Pearson et al. (2004) and the present study suggest that during peridotite-silicate melt partitioning, Pd and Pt behave as incompatible elements. Positive slopes of correlations in the Pd/Ir–Al_2O_3 and Re/Os–Al_2O_3 diagrams suggest that, in most cases, Pd and Re behave incompatibly, similar to Al. A shallow slope in the Pt/Ir–Al_2O_3 diagram (Fig. 6a) indicates that at low to moderately high degrees of partial melting, Pt is less incompatible than Pd, Re and Al. The slopes of correlations in Figs. 5–7 and the relative depletions observed in harzburgites (Fig. 8a) and depleted lherzolites require $D_{Re}^{s/l} < D_{Pd}^{s/l} < D_{Pt}^{s/l} < 1$ for peridotite-melt partition coefficients. This compatibility sequence is also consistent with the relative enrichment of these elements in metasomatized harzburgites (Fig. 8b, and Pearson et al., 2004)
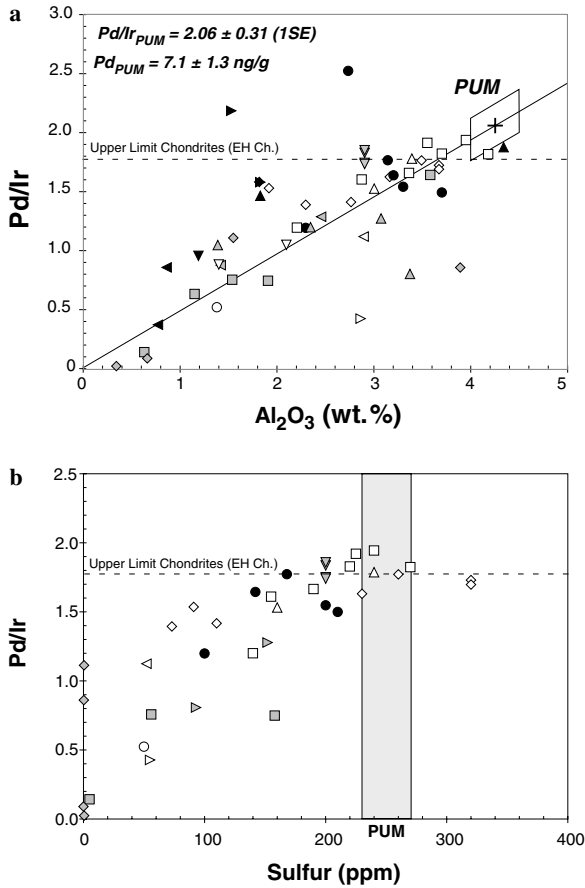
Fig. 7. (a) Pd/Ir–Al_2O_3 diagram. The good positive correlation suggests that Pd is incompatible, similar to Re (Fig. 5b). A few samples display elevated or reduced Pd/Ir relative to the correlation. The Pd/Ir$_{PUM}$ estimate lies outside the limit for chondrites as defined by EH chondrites (Horan et al., 2003). (b) Pd/Ir-S diagram. The correlations in (a) and (b) suggest that sulfide and incompatible HSE abundances in the peridotites are linked to the inventory of lithophile elements such as Al. This implies they are principally controlled by melt extraction and silicate melt metasomatism.
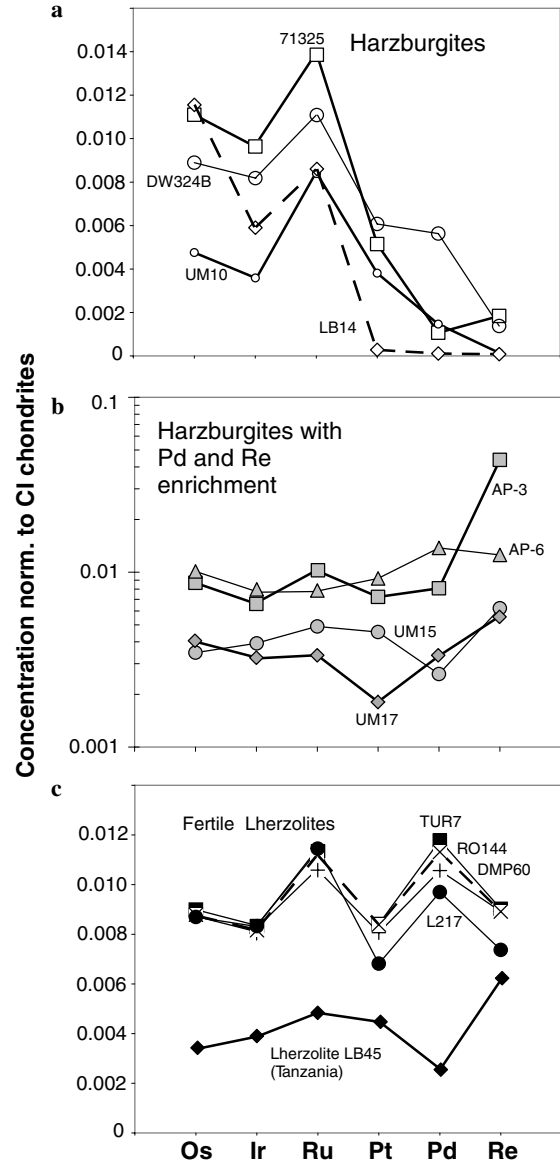

Fig. 8. Concentration diagrams for selected peridotites normalized to the mean of CI chondrite data of Horan et al. (2003). In (b) logarithmic scale is used because of large concentration ranges for incompatible HSE. For clarity, the sequence of elements follows that of increasing incompatible behavior during mantle melting from left to right. (a) Normal harzburgites showing depleted HSE patterns. (b) Harzburgites that show Pd and Re enrichments. (c) Fertile lherzolites. Sample LB45 shows anomalously low HSE abundances and Re enhancement. This sample may represent an example of refertilization via silicate melt (Chesley et al., 1999).

and in komatiites and basalts (Rehkämper et al., 1999b; Puchtel et al., 2004; Puchtel and Humayun, 2005). The incompatible nature of Pt and Pd in lherzolites and the sequence $D_{Re}^{s/l} < D_{Pd}^{s/l} < D_{Pt}^{s/l}$ are inconsistent with predicted peridotite-silicate melt partitioning of these elements, which are based on experimentally determined sulfide-silicate melt partition coefficients applied to peridotite melting models (Handler and Bennett, 1999; Lorand et al., 1999; Pearson et al., 2004). This discrepancy may be resolved if equilibrium between residual mono sulfide solid solution (mss) and Cu–Pt–Pd–enriched liquid sulfide controls HSE partitioning during peridotite melting (Bockrath et al., 2004). Two strongly depleted harzburgites from Tanzania (LB-14, KAT-1, Fig. 6a) show very low Pt/Ir and hint at a possible decrease of the bulk peridotite/melt partition coefficient for Pt at very high degrees of partial melting. The Pt/Os–Al_2O_3 diagram (Fig. 6b) is shown because of its importance for igneous Pt–Os fractionation processes in the mantle and the potential

for development of radiogenic ^{186}Os resulting from ^{190}Pt decay (Walker et al., 1997). Most samples are characterized by subchondritic or chondritic Pt/Os and are consistent with chondritic $^{186}Os/^{188}Os$ observed for upper mantle materials (Brandon et al., 2000; Walker et al., 2005). Only a few samples are characterized by suprachondric Pt/Os (LB45, UM15, UM19), mostly reflecting anomalously low Os abundances in these samples.

A negative correlation of Ir (also Ru and Os) with Al_2O_3 as found for the Pyreneean peridotites (see also data of

Lorand et al., 1999) and the data from Hannuoba, has also been observed at other locales (Pearson et al., 2004). It provides a good showcase of the effect of increasing degree of partial melting and associated mass loss on concentrations of compatible elements. The generally increasing scatter of compatible Ir-group PGE with increasing depletion may reflect increasing heterogeneity of the PGE carrier phases. This is witnessed in some Labait harzburgites by the presence of relatively large Ir-group PGE alloy nuggets (McDonough, personal communication) that, like in a NiS fire assay process, may result from coalescence of insoluble residual alloy phases. Such processes may also be responsible for occasionally high Ir-group element concentrations in depleted peridotites such as UM19. The increase of Os/Ir and Ru/Ir in some depleted harzburgites by up to a factor of 3 may signify a major change in the partitioning behavior of these elements at high degrees of partial melting.

Pearson et al. (2004) studied the HSE composition of a large number of refractory peridotites from various tectonic settings. They found that Os/Ir and Ru/Ir are within 30–50% of the CI chondrite value, with a few outliers to high and low ratios. Overall this behavior is consistent with previous HSE data on depleted peridotites (Pearson et al., 2004). High Os, Ir and Ru concentrations in komatiites indicate that at the high degrees of partial melting (30–40%) under which these magmas formed, these elements are less compatible than at lower degrees of melting (Brügmann et al., 1987; Rehkämper et al., 1999b, Puchtel et al., 2004; Puchtel and Humayun, 2005). This should manifest itself in lower Os, Ir and Ru concentrations in the residues, but might not always be resolvable because of associated effects from mass loss and increased heterogeneity. At present, it is difficult to assess why Os/Ir and Ru/Ir show more scatter in harzburgites than in lherzolites. In some cases anomalous ratios are associated with anomalously high (UM19) or low (UM10, UM17) concentrations of all Ir-group PGE, however, this is not always the case (samples KAT-1, 86-V2, AP-6). The possibility that digestion problems could afflict Os–Ir–Ru alloy-bearing refractory harzburgites cannot be excluded at present, since only limited data on the reproducibility of harzburgite standard reference materials are available (Meisel and Moser, 2004). A rigorous discussion of this issue is beyond the scope of the present work. More data are needed to substantiate the compatibility sequence and what controls fractionation of Ir-group PGE.

5.2. Redistribution of HSE by secondary processes

Before abundances of the HSE in PUM can be derived, the influence of processes other than partial melting on HSE abundances of peridotites must be evaluated. The data in Figs. 5–7 show some deviations of samples from correlations, almost certainly reflecting secondary processes. These processes may affect compatible and incompatible HSE.

5.2.1. Serpentinization and weathering

The extent to which the HSE in peridotites can be affected by surface processes remains poorly constrained. A strong argument against significant addition of radiogenic crustal Os during serpentinization is provided by good correlations of $^{187}Os/^{188}Os$ with Al_2O_3 for suites of highly serpentinized peridotites (this work Fig. 5a; Reisberg and Lorand, 1995). These correlations are generally accepted to be of igneous origin, reflecting the time-integrated effect of variable extent of depletion on a suite of genetically related peridotites. The argument for undisturbed $^{187}Os/^{188}Os$ systematics in some suites of peridotites derives from the observation that Al is rather immobile during aqueous alteration processes (Staudigel et al., 1996; Snow and Dick, 1995) and, as a consequence, correlations of Al with other moderately incompatible elements are often well preserved in serpentinized peridotites. Osmium and Al are chemically so different that they should behave in contrasting ways during alteration. Hence, secondary mobilization of Al or significant addition of radiogenic Os should result in degradation or obliteration of $^{187}Os/^{188}Os$–Al_2O_3 correlations of igneous origin. Roughly constant Os/Ir and Ru/Ir (Figs. 3 and 4) in a wide variety of samples showing little to extensive serpentinization (>10 wt% H_2O) support the notion that Os, Ir and Ru abundances in most of these samples were not or only slightly affected by serpentinization, weathering or other near-surface processes such as post-eruptive oxidation of sulfides in xenoliths. The good correlations of Re/Os and Pd/Ir with Al_2O_3 also suggest, at least for the majority of the samples, no or only limited influence of alteration processes on Re and Pd abundances. The effects of intense weathering may not show up in the present sample suite because visibly weathered material was excluded.

5.2.2. Melt percolation and metasomatism in the mantle

Many whole rocks of fertile lherzolites show an enhancement of Pd relative to Ir when normalized to carbonaceous chondrites, and it has been debated whether this might be a primary feature of the Earth's mantle or reflect secondary igneous processes (Pattou et al., 1996; Rehkämper et al., 1999a, Lorand et al., 1999, 2000; Alard et al., 2000; Schmidt et al., 2000; Morgan et al., 2001; Schmidt, 2004; Pearson et al., 2004). The new Pd/Ir data obtained by high-T Carius tube digestion on samples analyzed previously by NiS fire assay techniques are now much closer to chondritic values, supporting the view that some of the high Pd/Ir of peridotites from earlier NiS fire assay work may be analytical artifacts (Morgan et al., 2001; Gros et al., 2002). Yet the high-T Carius tube data still show slightly suprachondritic Pd/Ir in the most fertile lherzolites, consistent with previous results obtained by low-T Carius tube digestion (Rehkämper et al., 1999a; Handler and Bennett, 1999; Pearson et al., 2004). In fertile lherzolites, Pd/Ir is typically 42–52% higher than in CI chondrites, and about 10–20% higher than in EH chondrites, which show the highest Pd/Ir of all chondrite groups (up to

40% higher than CI, Horan et al., 2003). In this section, evidence for mobilization of HSE in peridotites by igneous processes in mantle will be discussed, including potential roles for fluid metasomatism, sulfide melt mobility, and refertilization by silicate melt and solid state mixing.

Osmium isotopic studies and micro distribution studies of PGE in sulfides have revealed significant compositional and isotopic heterogeneity of sulfides in mantle peridotites. It has been observed that Cu–Pd–Pt-rich sulfides tend to occur preferentially along silicate grain boundaries in peridotites, while presumably primary Ni-rich sulfides occur preferentially included in silicates (Burton et al., 1999; Alard et al., 2000, 2002; Luguet et al., 2003). Such bimodal characteristics of sulfides in peridotites may be a common feature in oceanic and continental environments. These variations were interpreted in terms of metasomatic addition of Pd- and Pt-enriched sulfides along grain boundaries by percolating sulfide or silicate melts, fluids, or incomplete extraction of silicate melt (Alard et al., 2000, 2002; Luguet et al., 2003). Good correlations between incompatible HSE with lithophile fertility indicators such as Al_2O_3 (Figs. 5–7) suggest that the bulk HSE budget in most peridotites has been little affected by sulfide melt or fluid mobility. Positive correlations between Pd/Ir with Al_2O_3 and S (Fig. 7) and, hence, of sulfur abundances with Al_2O_3 are also inconsistent with the view that the HSE composition of peridotite whole rocks were significantly modified by percolation of sulfide melt. Recent experimental work indicates that during melting of peridotite, Cu, Pt, Pd and Re dissolve in sulfide melt, while compatible PGE are largely retained in residual Ni–Os–Ir–Ru-enriched mss or alloys (Bockrath et al., 2004). Once silicate melt crystallizes in the mantle or is extracted incompletely, it will precipitate Cu–Pt–Pd–Re-rich sulfide, leading to two types of sulfides in melting residues and melt pathways in the mantle, thus providing for the possibility of metasomatic re-enrichment of melt residues with incompatible HSE.

In order to evaluate potential effects of metasomatism on bulk rocks more rigorously, abundances of all incompatible HSE, along with Os isotopic compositions, need to be taken into account. Because Re is more depleted in harzburgitic melting residues than Pd (Fig. 8a), Re must be somewhat more incompatible than Pd. This conclusion is supported by data from other studies (Handler and Bennett, 1999; Pearson et al., 2004). Hence, any igneous enrichment of Pd relative to Ir in fertile peridotites should be accompanied by even stronger enrichment in Re, and to lesser extent Pt. In this context it is instructive to study depleted samples that show evidence for metasomatic addition of incompatible HSE. Some harzburgites and depleted lherzolites from ophiolites show such features in the form of radiogenic $^{187}Os/^{188}Os$ and higher than expected abundances of Pt, Pd and Re (Figs. 5–8, this work; Büchl et al., 2002), In the $^{187}Os/^{188}Os$–Al_2O_3 diagram (Fig. 5a) most sample suites define positive correlations with the slopes of different suites of samples depending on the age of melt extraction (Reisberg and Lorand, 1995; Meisel

et al., 2001). Some depleted samples, however, plot off these correlations, typically toward higher $^{187}Os/^{188}Os$, suggestive of the addition of radiogenic Os *via* melt percolation. These samples include 71,322 from Lherz and LB-4 from Tanzania, the latter also showing Pt and Pd enhancement. Other depleted peridotites, such as those from Troodos, show field relations, fractionated HSE patterns, and evidence for the addition of radiogenic Os that are believed to have formed in the proximity of melt percolation channels (Büchl et al., 2002). Abyssal peridotites from the Kane Fracture Zone (AP-3 and AP-6, Fig. 8b) also show anomalously high abundances of incompatible HSE at low Al_2O_3. The relative enrichment in such cases is almost always Re > Pd > Pt (for more examples see Pearson et al., 2004), presumably because that represents the sequence of enrichment in the melts that reacted with the peridotite, in accordance with the different partition coefficients of these elements.

While the correlations of $^{187}Os/^{188}Os$, Re/Os, Pt/Ir, Pd/Ir, Pt/Os and Pd/Os with Al_2O_3 in many peridotites are consistent with variable degrees of partial melting, it should be noted that, in principle, they could also have been produced by refertilization of depleted peridotites by silicate melts. Refertilization has been invoked to explain major and minor element correlations in peridotite suites (Elthon, 1992) and may occur in response to cooling of melts migrating into lithospheric mantle and saturation in pyroxenes, spinel or garnet. If co-precipitation of sulfides from melt occurs, this may lead to concurrent addition of incompatible HSE, along with moderately incompatible lithophile elements like Al and Ca. Refertilization may be a viable process for some samples that plot off correlations between Pd/Ir, Pt/Ir and Al_2O_3, and show evidence for the addition of radiogenic Os via silicate melt. Such samples include LB-4 and LB-45 from Tanzania (Fig. 8c, Fig. A3; Chesley et al., 1999), lherzolite xenoliths from Vitim (Pearson et al., 2004) and possibly some samples from the UM suite of peridotites (this work, Table 3; Morgan, 1986). Other sample suites, however, are difficult to explain by this process. The negative Ir–Al_2O_3 correlation for the Pyrenean peridotites (Fig. 2) suggests a mass loss effect that can be modeled via melt extraction. Refertilization through percolating silicate melt is much more difficult to reconcile with this observation, because mass and volume proportions of phases added would have to mimic those during melting and concurrent variations in porosity quite accurately.

Fertile lherzolites show slightly suprachondritic Pd/Ir, Pd/Pt and Pd/Re. This feature appears in xenolith and massif-type peridotites and, with few exceptions, appears to be a global feature of the lithospheric mantle (Schmidt et al., 2000; Morgan et al., 2001; Schmidt, 2004). In contrast, Re and Pt abundances are not appreciably enhanced in fertile lherzolites relative to Ir and Os (Figs. 5b, 6, 8c, Handler and Bennett, 1999; Rehkämper et al., 1999a; Pearson et al., 2004), consistent with the observation that fertile lherzolites typically possess chondritic $^{187}Os/^{188}Os$ (Fig. 5a

and Meisel et al., 2001). If metasomatic processes were responsible for the Pd enhancement in fertile lherzolites, Re should be enriched relative to Pd or Pt (Fig. 8c), but, with one exception (sample TA15), this is not observed. The sequence of relative enrichment of Re > Pd > Pt in metasomatically affected depleted peridotites contrasts with HSE patterns of fertile lherzolite (Fig. 8). Among samples that define the straight correlation between Pd/Ir and Al$_2$O$_3$ in Fig. 7a, those from Lanzo and the Pyrenees belong to the LREE-depleted peridotite varieties at these locales (Lorand et al., 1993, 1999, 2000). These peridotites are also characterized by positive $\varepsilon_{Nd} > 8$, not unlike the MORB mantle source. Peridotite-melt partition coefficients of Re, Al, and the heavy REE are similar (Morgan, 1986). For this reason, it would be rather difficult to enhance these elements (and Pd, which is even more compatible) by metasomatism, but not the LREE with one or two orders of magnitude lower bulk partition coefficients. Consequently, the straight correlations defined by these particular sample suites are very difficult to reconcile with silicate melt percolation processes in the lithosphere.

Stochastic solid-state mixing of recycled oceanic lithosphere and convecting mantle represents another process that may control abundances of incompatible HSE in peridotites. Straight correlations of ^{187}Os/^{188}Os, Re/Os, Pd/Ir and Pt/Ir with Al$_2$O$_3$ (this work Figs. 5–7; Reisberg and Lorand, 1995; Meisel et al., 2001; Saal et al., 2001; Reisberg et al., 2005) could reflect ancient depletion events in harzburgites and locally homogenized layers of former oceanic crust and mantle lithosphere converted to lherzolites. Some evidence is consistent with solid state mixing in the mantle: (1) grain- to outcrop-scale Os isotopic heterogeneity in peridotites (Burton et al., 1999; Alard et al., 2002; Meibom et al., 2002), (2) evidence for ancient melting events from ^{187}Os/^{188}Os data in peridotites and Os–Ir alloys derived from the convecting mantle (Parkinson et al., 1998; Brandon et al., 2000; Meibom et al., 2002) (3) heterogeneous sulphide populations (Alard et al., 2000), (4) fertile lherzolites showing LREE depletion and absence of metasomatic features (Pyrenees, Lanzo), and (5) possibly global HSE characteristics of fertile lherzolites such as chondritic ^{187}Os/^{188}Os, invariant Os/Ir and Ru/Ir, and, high Pd/Ir and Pd/Pt.

5.3. HSE composition of PUM

As outlined in the previous sections, the behavior of the HSE in the majority of samples of the present work can be understood in terms of silicate melt extraction, solid-state mixing of recycled lithosphere, and in some cases silicate melt percolation. Our data indicate chondritic Os/Ir in PUM, but a Ru/Ir ratio that is ~30% higher than in chondrites. Suprachondritic Ru/Ir in peridotites have been noted before (Schmidt et al., 2000). But previous work displayed a great deal of variation from subchondritic to suprachondritic compositions that did not permit an unambiguous assessment of this issue (Pattou et al., 1996;

Rehkämper et al., 1999a; Handler and Bennett, 1999; Lorand et al., 1999, 2000). Only three depleted samples in the present study, KAT-1, AP-6 and UM17 show chondritic Ru/Ir. Judging from the HSE patterns of these samples (Fig. 8) it is more likely that Ru/Ir in these samples has been affected by igneous processes, rather than representing typical upper mantle compositions. Similar chondritic Ru/Ir ratios were reported in harzburgites by Pearson et al. (2004). Given the homogeneity of Ru/Ir in fertile lherzolites observed in the present study, there is little doubt that Ru/Ir$_{PUM}$ must be suprachondritic (see also Beni Bousera lherzolite data in Pearson et al., 2004). Aside from igneous processes, the non-systematic scatter in Os/Ir and Ru/Ir observed here and elsewhere might still reflect occasional incomplete digestion. This possibility needs to be kept in mind because reproducibility has not been tested rigorously for harzburgites. Extreme fractionation of Ir, Os and Ru were reported from replacive dunites from the Troodos ophiolite (Büchl et al., 2002), and are almost certainly not representative of the upper mantle. The HSE composition of many depleted abyssal peridotites also may have been affected by melt percolation because they also sample the upper portion of the melting column underneath ocean ridges. Hence, abyssal peridotites may show more heterogeneity of ratios involving Os, Ru and Ir than fertile peridotites. Because Ir is a compatible element that shows comparatively low variance in lherzolites, and the upper mantle has a composition corresponding to fertile lherzolite (McDonough and Sun, 1995), the Ir abundance of PUM has been known reasonably well (Morgan et al., 2001). Concentrations of Ir, Ru and Os tend to increase with increasing degree of partial melting (as observed in Pyrenean peridotites, Fig. 2), hence, we rely exclusively on lherzolites for the calculation of Ir-group PGE abundances in PUM (Fig. 9). For consistency, we only use data obtained by high-temperature digestion for constraining PUM. Among lherzolite HSE data obtained by isotope dilution and low-temperature Carius tube digestion, three lherzolites from Beni Bousera (Morocco) yield results that are comparable to the present work, while lherzolites from Vitim (Pearson et al., 2004), the Cameroon line (Rehkämper et al., 1997) and E-Australia (Handler and Bennett, 1999) show variability that may reflect secondary processes.

The mean Ir concentration of 28 lherzolites from the present work with >2 wt% Al$_2$O$_3$ yields Ir$_{PUM}$ = 3.5 ± 0.4 ng/g (1σ) or 0.0080 ± 0.0009*CI chondrites (using the mean of the CI data in Horan et al., 2003). This value is similar to previous estimates for PUM based on larger data sets of lherzolites (Fig. 9 and Morgan et al., 2001). Our cutoff value at 2 wt% Al$_2$O$_3$ excludes harzburgites that show larger variability in Ru/Ir and Os/Ir. Included in our calculation is the mean of the four UB–N analyses in Table 2. However, we excluded lherzolite samples 86-2, LB-45, UM-5, UM-14, UM-15 and UM-17 from Table 3, because of highly variable HSE abundances and ratios in these samples. Using Ir$_{PUM}$, the concentration of Os$_{PUM}$ (3.9 ± 0.5 ng/g, 1σ) is

determined from the mean Os/Ir_{PUM} of 1.12 ± 0.09 (1σ), which is obtained from the same set of lherzolites used to determine Ir_{PUM}. These lherzolites also yield a mean $Ru/Ir_{PUM} = 2.03 \pm 0.12$ (1σ) and $Ru_{PUM} = 7.0 \pm 0.9$ ng/g (1σ), respectively. The latter value is more than 20% higher than previous estimates.

PUM abundances for HSE that behave incompatibly during mantle melting (Pt, Rh, Pd, Re, Au) can be estimated, either from Al-rich lherzolites, or from correlations with moderately incompatible elements, such as Al or the heavy rare earth elements. Estimates for the Al_2O_3 content of PUM range between 4.0 and 4.5 wt% (McDonough and Sun, 1995). Hence, extrapolation of the correlations in Figs. 6a and 7a yield estimates for ratios of incompatible to compatible HSE in PUM. From these regressions, $Pt/Ir_{PUM} = 2.21 \pm 0.21$ (1σ) and $Pd/Ir_{PUM} = 2.06 \pm 0.31$ (1σ) were obtained, respectively, assuming Al_2O_{3PUM} of 4.25 ± 0.25 wt%. Samples that show anomalous abundance features of Ir-group HSE were excluded from these regressions. These estimates combined with Ir_{PUM} yield $Pt_{PUM} = 7.6 \pm 1.3$ ng/g (1σ), and $Pd_{PUM} = 7.1 \pm 1.3$ ng/g (1σ), respectively. The PUM value for Re is best estimated using the precise value for $^{187}Os/^{188}Os_{PUM}$ of 0.1296 ± 0.0008 from the study by Meisel et al. (2001). For $t = 4.56$ Ga, the ^{187}Re decay constant (Smoliar et al., 1996) and initial $^{187}Os/^{188}Os$ given in Shirey and Walker (1995), we obtain $Re/Os_{PUM} = 0.090 \pm 0.002$ and $Re_{PUM} = 0.35 \pm 0.06$ ng/g. This value agrees within error with less precise estimates based on Re/Os- or Re/Ir–Al_2O_3 correlations. Our new estimates for Ru, Pt, Pd and Re in PUM are significantly higher than previous estimates that were based on data of variable quality (Morgan et al., 2001).

Rhodium was not analyzed in the present study. The mean Rh/Ir of fertile lherzolites from the Pyrenees is chondritic (0.32 ± 0.03, Lorand et al., 1999). Even though we have no new data for gold, some of the samples in the present study were analyzed previously for Au by ICPMS and NAA (Lorand et al., 1993, 1999, 2000). When combined

with the new Ir data, a relatively imprecise Au/Ir_{PUM} of 0.55 ± 0.15 (1 s) yields $Au_{PUM} = 1.9 \pm 0.6$ ng/g.

The Re/Os_{PUM}, Pt/Ir_{PUM} and Pt/Os_{PUM} ratios are chondritic, consistent with evidence from $^{187}Os/^{188}Os$ and $^{186}Os/^{188}Os$ systematics of materials derived from the upper mantle (Brandon et al., 2000; Meisel et al., 2001; Walker et al., 2005). Pd/Ir_{PUM} appears to be slightly suprachondritic and overlaps with values in EH chondrites (Horan et al., 2003). The range of Pd/Pt in fertile lherzolites (0.80–0.92) also overlaps with the range of values for EH chondrites (Pd/Pt = 0.74–0.87) and extends to suprachondritic values, indicating that Pd is enriched relative to other HSE. Precise HSE data on komatiites also suggest that Pd/Pt in the mantle sources of komatiites is slightly suprachondritic (Puchtel et al., 2004; Puchtel and Humayun, 2005), and thus supports the notion that Pd enhancement in Earth's mantle may be a global feature and is not restricted to lithospheric mantle only. Morgan et al. (2001) pointed out that some lherzolites do not show the Pd enhancement that seems to typify other fertile mantle lherzolites (see also Rehkämper et al., 1997). Some of the Kilbourne Hole samples, for example, are anomalous, in that they have subchondritic Os/Ir (Morgan, 1986) and the low Pd/Ir may be caused by enhanced Ir contents, rather than low Pd. A reassessment of the heterogeneity of HSE distribution in "anomalous" peridotites as potentially reflecting preserved primordial heterogeneities (Morgan et al., 2001) will require analysis using high-temperature digestion techniques. In the present work, heterogeneity is somewhat more prevalent in depleted samples (Figs. 2–7), and, in most cases, can be explained by igneous processes.

5.4. HSE abundances of PUM and the influence of fractionation processes involving metal

The combination of chondritic relative abundances for some HSE (Re, Os, Ir, Pt) and suprachondritic abundance ratios involving Ru and Pd presents a challenge for any of the conceptual models proposed previously to explain the HSE characteristics of the Earth's mantle. The difficulties involving silicate-sulfide partitioning during metasomatism to explain HSE ratios in the new PUM estimate were outlined in the previous sections. Here, we briefly evaluate whether the observed fractionations can be generated by metal-silicate and solid metal-liquid metal partitioning. Pressure- or temperature-dependent variations of metal-silicate partition coefficients are difficult to evaluate because experimental data are lacking for some HSE and existing data are not sufficiently accurate and precise to be employed for modeling of HSE patterns in mantle residues after core formation (Righter et al., 2000; Holzheid et al., 2000; Ertel et al., 2001). The absence of primary Fe–Ni metal and the relatively oxidized composition of upper mantle peridotites suggest that no metal remained in the mantle, presumably because of large-scale melting and deformation-assisted segregation during core formation (Minarik et al., 1996; Ballhaus and Ellis, 1996; Rushmer
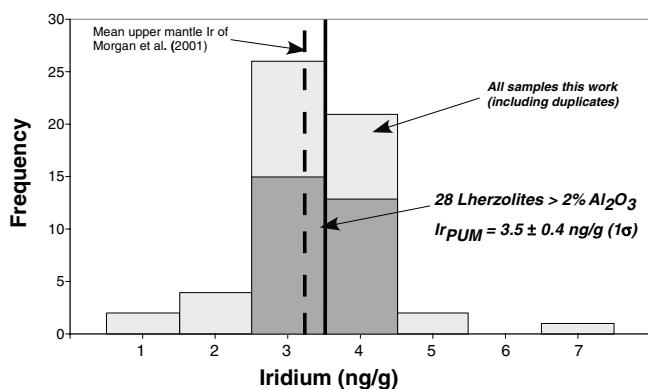
Fig. 9. Histogram plot of Ir concentrations in peridotites from the present study (light gray). Dark gray are data for lherzolites with $Al_2O_3 > 2$ wt% that are used for calculation of the mean Ir concentration in PUM. A previous estimate for Ir_{PUM} from Morgan et al. (2001) is shown for comparison.

et al., 2000). More recent data suggests that metal may indeed coexist with perovskite and ferropericlase in the lower mantle (Frost et al., 2004), but, it is unknown if such metal is relict of the metal that formed the Earth's core. If metal was superheated during core formation, liquid metal trapped in silicates should have a composition similar to the integrated composition of metal and sulfide phases in the building blocks of the planet. Because the latter are believed to be broadly chondritic, the final result may be hard to distinguish from that of a chondritic late veneer.

Alternatively, partitioning of HSE between solid metal and liquid metal may have affected the HSE pattern of Earth's mantle. HSE data in some previous studies on oceanic peridotites show suprachondritic Pt/Ir and Pd/Ir, and were interpreted in terms of a small contribution of material from the outer core entrained in lower mantle and transported to the upper mantle by convection (Snow and Schmidt, 1998). Subsequent work did not confirm suprachondritic Pt/Ir in abyssal peridotites, and the elevated Pd/Ir in some of these rocks were interpreted to reflect metasomatic processes (Rehkämper et al., 1999a). The present study supports the view that upper mantle peridotites generally do not possess suprachondritic Pt/Ir or Pt/Os. Chondritic $^{186}Os/^{188}Os$ in abyssal peridotites also indicate that these materials have not experienced long-term Pt enrichment (Brandon et al., 2000). Furthermore, contributions from the liquid outer core could have imposed chondritic proportions of HSE only prior to inner core crystallization. For illustrative purposes, a model for the evolution of HSE ratios in the residual liquid during crystallization of a planetary inner core is shown in Fig. 10a. Absolute values of solid metal-liquid metal partition coefficients ($D^{sm/lm}$) are strongly dependent on the minor element composition of the core (Jones and Malvin, 1990; Walker, 2000; Chabot et al., 2006), which, in the Earth's case, is not well known. Work on magmatic iron meteorite groups indicates limited variation of ratios of $D^{sm/lm}$ during the early stage of metal fractionation (Pernicka and Wasson, 1987; Hoashi et al., 1993; Morgan et al., 1995; Wasson, 1999). Consistent sets of $D^{sm/lm}$ values for HSE can be obtained from these studies. Although the $D^{sm/lm}$ values used in Fig. 10 were derived from processes that occurred at relatively low pressures, experiments at high pressures and temperatures suggest similar ratios of $D^{sm/lm}$, at least for the elements Pt, Re, and Os (Walker, 2000). In Fig. 10, $D^{sm/lm}$ estimated for initial metal fractionation in the IIIAB iron parent body were employed. The results show that Pd/Ir, Pt/Ir, Pt/Os, Ru/Ir and Re/Os in residual liquid metal quickly become suprachondritic, whereas Os/Ir in the liquid becomes subchondritic (Fig. 10a). These relationships are inconsistent with chondritic Re/Os, Pt/Os and Os/Ir in PUM, hence contamination of the upper mantle with somewhat evolved liquid core remains an unlikely proposition. Alternatively, solid metal may be retained in the mantle residue in cases where liquid metal is not superheated and drains into the core. The composition of early fractionated solid metal is displayed in Fig. 10b,
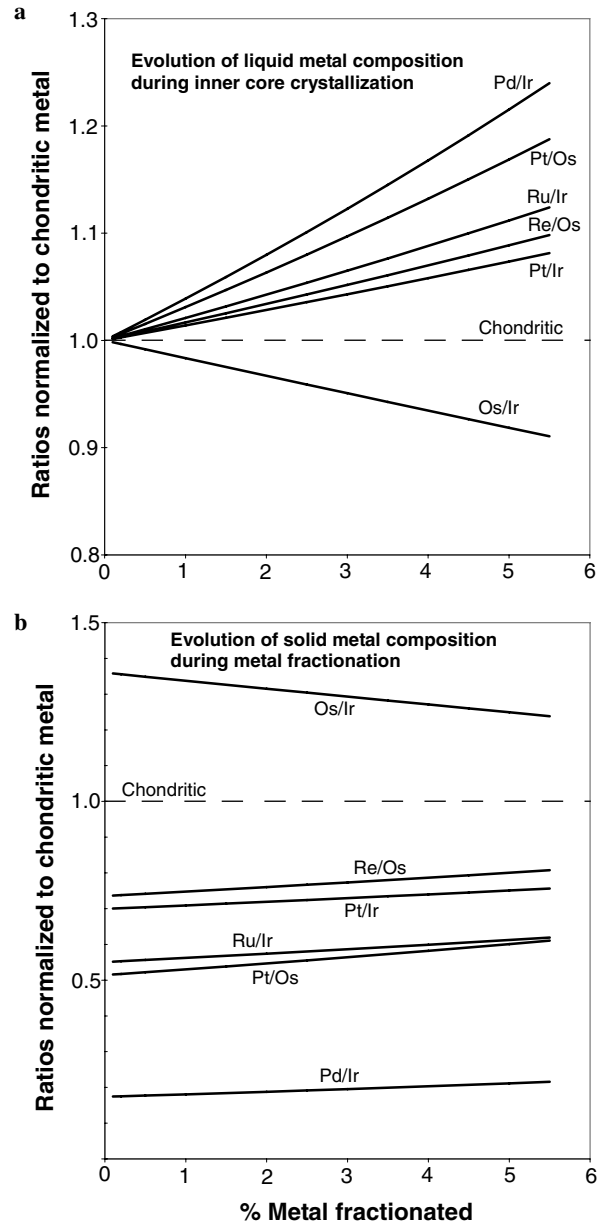

Fig. 10. Evolution of HSE ratios in liquid and solid metal during the early stages of Rayleigh fractional crystallization of a solid asteroidal core. Values for ratios are shown up to 5.5% metal fractionated, the mass fraction of the Earth's inner core. The data are normalized to the chondritic starting composition of the metal (assuming 0.26 ppm Re; 3 ppm Os; 2.7 ppm Ir; 4.15 ppm Ru; 5.5 ppm Pt; 3.15 ppm Pd). A consistent set of solid metal-liquid metal partition coefficients was used: $D^{sm/lm}_{Ir} = 4.6$; $D^{sm/lm}_{Os} = 6.3$; $D^{sm/lm}_{Ru} = 2.5$; $D^{sm/lm}_{Pt} = 3.2$; $D^{sm/lm}_{Pd} = 0.8$; $D^{sm/lm}_{Re} = 4.6$. These values are based on estimates for the initial crystallization conditions of the core of magmatic IIIAB iron meteorites (Pernicka and Wasson, 1987; Hoashi et al., 1993; Wasson, 1999). For details see text. This example illustrates that bulk contamination of the mantle with small amounts of outer core likely would have produced non-chondritic HSE ratios in the mantle (a). The same is true for solid metal that may have been retained in the mantle during metal-silicate segregation (b).

using the same $D^{sm/lm}$ as in Fig. 10a. Early crystallized metal shows distinctly non-chondritic HSE ratios, inconsistent with the PUM data. In conclusion, none of the processes

involving metal-silicate or solid metal-liquid metal partitioning yields HSE fractionations that provide a suitable fit to the PUM data.

5.5. Comparison with chondrites and lunar impact breccias

We now evaluate the late veneer-hypothesis in light of the new data for PUM. Representative HSE analyses of chondrites from various groups are compared to PUM in Fig. 11. None of the chondrites provides a good match for the PUM pattern. Ordinary chondrites, while possessing the right Re/Os, are depleted in Pd. EH chondrites are nearly, but not quite as enriched in Pd as PUM, but have lower Re/Os. None of the chondrites show the extent of Ru enhancement found for PUM. In Fig. 12, Pd/Ir and Ru/Ir are plotted vs. ^{187}Os/^{188}Os, a proxy for Re/Os. These diagrams show that PUM defines a unique composition distinct from any of the hitherto analyzed chondrite groups. The patterns in Fig. 11 suggest that PUM is enriched in HSE having moderately volatile behavior under reducing conditions. Recently, Schmidt (2004) proposed that the volatile and refractory siderophile element pattern of the Earth's mantle may reflect late accretion of primitive material with enhancement of volatile elements. This hypothesis, however, does not provide a simple explanation for the very disparate level of enrichment of volatile elements such as Ge and S, nor for the enrichment of Ru over other refractory siderophiles such as Ir, Os and Pt in the Earth's mantle.

Further constraints on the viability of the late veneer hypothesis for the HSE composition of PUM can potentially be obtained from lunar materials. The presence of numerous large impact basins and craters attests to the fact that the Moon underwent severe bombardment by large objects, subsequent to the 4.5–4.3 Ga formation of the lunar highlands. The Moon has been tectonically inactive for most of its history. Consequently, lunar rocks that contain meteoritic components can be used to constrain the characteristics of the planetesimals that impacted the Moon early in its history (Hertogen et al., 1977). Precise HSE data obtained on 3.89 Ga old lunar impact melt breccias from the Serenitatis impact basin sampled by Apollo 17 (Norman et al., 2002) represents a new opportunity for detailed comparisons with terrestrial data. These impact melt rocks show enhancement of Pd and Ru relative to other HSE and provide the best match to the HSE pattern of PUM (Fig. 13). HSE in these samples are extremely well correlated with each other, suggesting they represent binary mixtures of a high-HSE component, presumably a LL or EH chondrite-like impactor (James, 1995; Norman et al., 2002; Tagle, 2005), and a component characterized by low HSE abundances. It is the low-HSE component that is characterized by enhanced Pd/Ir, Pd/Pt, Ru/Ir (Fig. 14) and thus is producing PUM-like HSE patterns in the mixtures (Fig. 13). The exact composition and origin of the low-HSE mixing end member are not well constrained. Traditionally, such low-HSE mixing end members
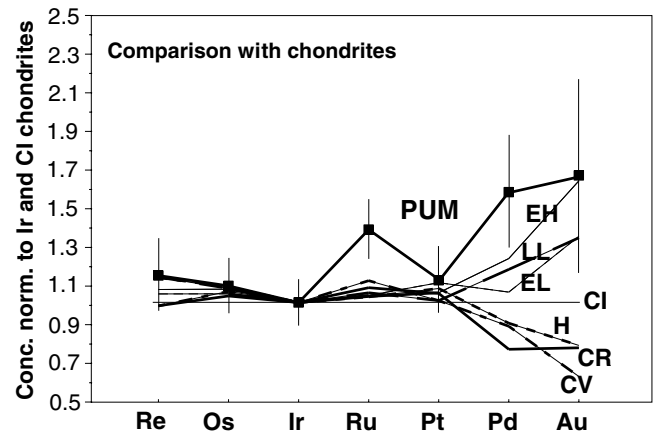

Fig. 11. Double-normalized concentration diagram (normalized to Ir and the mean of CI chondrite data of Horan et al., 2003) showing representative HSE patterns of chondrites from various groups and PUM. Note that, in contrast to Fig. 8, the scale is linear and the elements are arranged from left to right with increasing volatility, following cosmochemical convention. For the Au concentration estimate of PUM, see text. The Au data on chondrites are published neutron activation data from the literature. None of the known chondrite groups provides a good match to PUM.
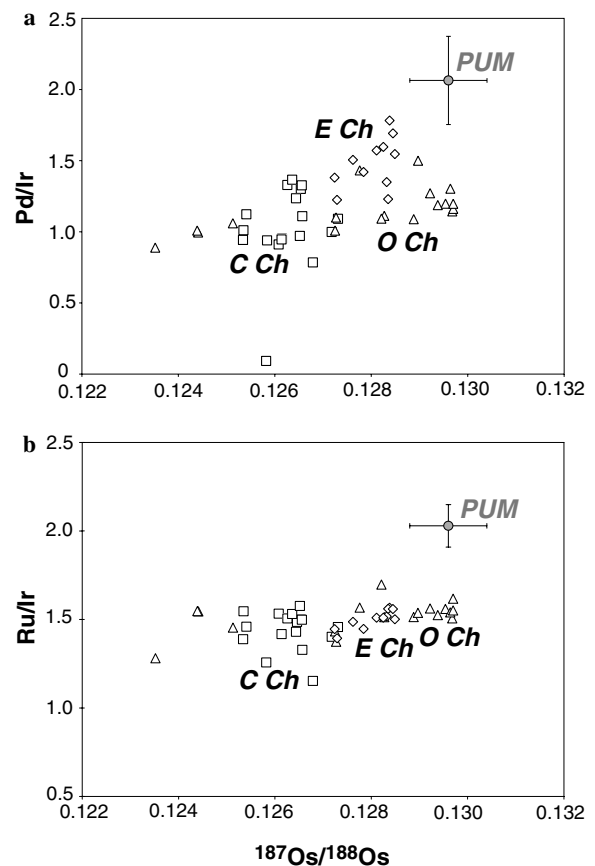

Fig. 12. Ratio diagrams, highlighting the distinct composition of PUM (this work, gray circle with 1σ uncertainties) and chondrites (Walker et al., 2002; Horan et al., 2003). Squares, carbonaceous chondrites; triangles, ordinary chondrites; diamonds, enstatite chondrites. ^{187}Os/^{188}Os reflects the time-integrated Re/Os of these samples.

in lunar impact rocks have been interpreted as representing the indigenous HSE composition of lunar igneous rocks (Hertogen et al., 1977; James, 1995; Norman et al., 2002). Indigenous Ir-group PGE abundances of lunar igneous rocks are mostly very low (Wolf et al., 1979; Righter et al., 2000; Walker et al., 2004). Extrapolation of the melt rock data to very low Ir abundances, for example 20 ppt Ir, yields suprachondritic HSE/Ir ratios, yet an enrichment sequence (Ir ≪ Pt < Ru < Re < Pd) that is different from HSE patterns of terrestrial mafic igneous rocks. An alternative explanation for the low-HSE mixing end member would be that it reflects a second meteoritic component with a unique composition (Norman et al., 2002). Studies of pristine lunar highland samples may provide additional constraints regarding the nature of the low-HSE end member in lunar impact rocks.

6. Late accretion of the Earth–Moon system and the HSE budget of the silicate Earth

Because the Moon is a one-plate planetary body, the lunar crust provides a record of processes that must have affected early Earth as well, whose early record has long been obliterated prior to plate tectonics. Because of their proximity, the Moon and Earth almost certainly sampled the same populations of projectiles since formation of the Moon by a giant impact (Hartmann et al., 2000), with Earth receiving much more material than the Moon because of the larger gravitational cross section (Chyba, 1991; Hartmann et al., 2000; Morgan et al., 2001). Similar HSE characteristics of lunar impact breccias from the Apollo 17 site and PUM strengthens the case that the HSE inventory of PUM may have been produced by late accretion 4.5–3.8 Ga ago (the late veneer hypothesis). It implies that, in spite of lack of direct evidence for meteorite
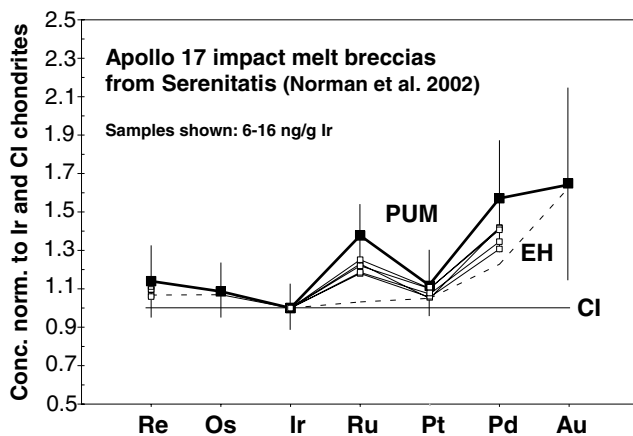

Fig. 13. Double-normalized concentration diagram (see Fig. 10) showing HSE pattern of PUM compared to some lunar poikilitic impact melt rocks (open squares) from the Apollo 17 landing site near the Serenitatis impact basin (Norman et al., 2002) and a typical EH chondrite (dashed line, Horan et al., 2003), which shows Pd enhancement, but no Ru enhancement. The lunar impact melt rocks also display Ru and Pd enhancements and provide the best match with the PUM pattern.
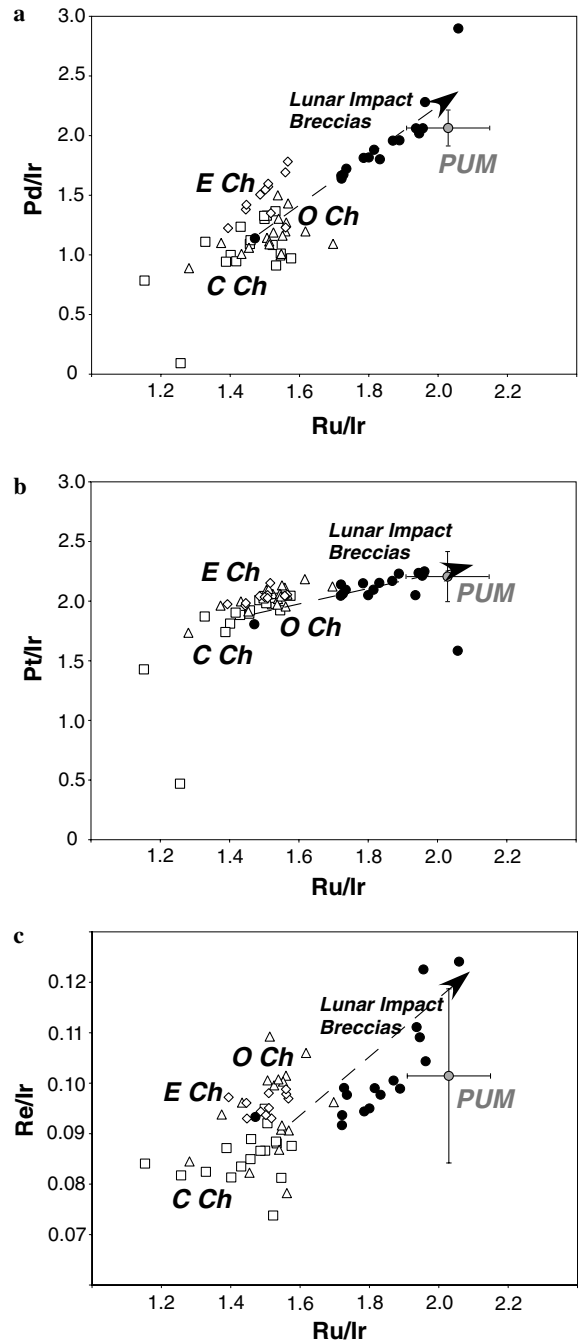

Fig. 14. Diagrams illustrating the mixing relations for Apollo 17 lunar impact melt rocks from Serenitatis (Filled circles. Data from Norman et al., 2002). Symbols and data sources as in Fig. 12. The breccias contain a chondritic component, similar to LL or EH chondrites (James, 1995; Morgan et al., 2001; Tagle, 2005). A second component is characterized by suprachondritic Ru/Ir and Pd/Ir. PUM is located close to the mixing lines (arrows) defined by the impact melt rocks.

contamination in early Archean crustal materials (Ryder et al., 2000; Anbar et al., 2001), meteorite-contaminated material must have occurred on Earth prior to 3.8 Ga. Consequently, such meteorite-contaminated early crust must have been returned to the Earth's mantle by some type of Hadean recycling. As the PUM composition lies

in or near the continuity of the mixing lines for HSE ratios in the lunar impact melt rocks (Fig. 14), it is very likely that the HSE pattern of PUM also reflects the presence of two or more major components. A chondritic component may have been delivered before and during the course of the late heavy bombardment. Another component is required to explain enhanced Ru and Pd in PUM. This component may reflect an unknown type of igneous HSE fractionation in crustal material of the Hadean Earth. These fractionations may have been imposed on the silicate Earth and the Moon as a result of magma ocean processes following the giant impact that led to formation of the Moon. Alternatively, the HSE composition of PUM may have been affected by primitive meteoritic material of unique composition and unlike the chondrites found on the surface of the modern Earth.

Arguments based on crater diameter, impactor mass and impact velocity systematics require a Earth/Moon mass influx ratio between 30 and 53, although much higher estimates have been proposed as well (Chyba, 1991; Hartmann et al., 2000; Morgan et al., 2001). The total mass accreted to the lunar surface, based on cumulative mass estimates from the largest lunar basins, amounts to 1×10^{20} kg (Chyba, 1991; Morgan et al., 2001). This result and the estimated Earth/Moon influx ratio of 53 yield a maximum estimate for terrestrial late accretion of $3–5 \times 10^{21}$ kg or roughly 0.1% of the mass of the Earth. This estimate provides only enough material to account for the HSE inventory of the upper mantle. If the HSE PUM abundances are also typical of the lower mantle, then the Earth/Moon influx ratio must have been 4 times higher than estimated (Morgan et al., 2001). High HSE abundances of komatiites and picrites that may derive from lower mantle plumes (Brügmann et al., 1987; Brandon et al., 1999, 2003; Puchtel et al., 2004; Puchtel and Humayun, 2005), and evidence from seismic tomography for some form of whole mantle convection in the Earth (Tackley, 2000) hint that the HSE estimates for PUM may apply to most of the lower mantle as well. Accretion flux estimates during the Hadean eon are significantly influenced by the number of large objects (>100 km) that impacted the planets (Chyba, 1991; Morgan et al., 2001). Unfortunately, the statistics of very large basins (>1000 km diameter) in the inner solar system are not well constrained (Ryder et al., 2000; Hartmann et al., 2000). Only two such basins, Imbrium and South Pole-Aitken, have been clearly identified on the Moon. Several very large impacts are predicted for the early Earth if the PUM estimate applies to the whole mantle. If this is correct, some very large lunar basins may have escaped identification.

Acknowledgments

Appendix A. Comparison of results obtained by different digestion techniques

Comparison of Ru/Ir and Pd/Ir data obtained by isotope dilution and high-temperature Carius tube digestion (345 °C) with data obtained on the same samples by NiS fire assay and ICP-MS or NAA techniques is shown in Figs. A1 and A2. Data based on NiS fire assay digestion shows larger scatter, even though sample sizes generally have been larger (typically 10–15 g) compared with Carius tube digestion (typically 2–3 g). This suggests that heterogeneous distribution of HSE-bearing phases cannot account for the larger scatter in fire assay-based analyses (Meisel and Moser, 2004). Systematically lower abundances of refractory Ir-group PGE along with the increased scatter indicate that NiS fire assay-based techniques often do not access the complete inventory of Ir-group PGE (Morgan et al., 2001; Puchtel et al., 2004). Fire assay-based techniques tend to underestimate Ru/Ir, because Ru might
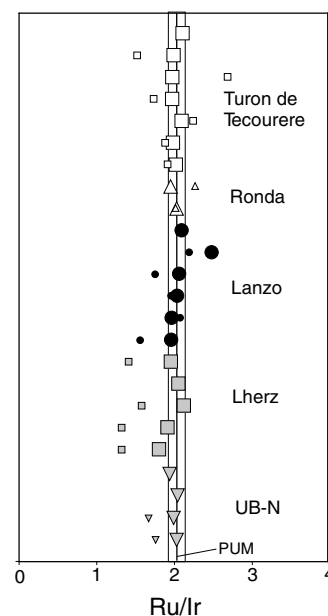

Fig. A1. Ru/Ir in samples analyzed by isotope dilution and high-temperature Carius tube digestion (large symbols, this work) compared with NiS fire assay-ICP-MS or NiS fire assay-NAA data (small symbols) on the same samples but different sample aliquots (data from Lorand et al., 1993, 1999, 2000; Snow and Schmidt, 1998).
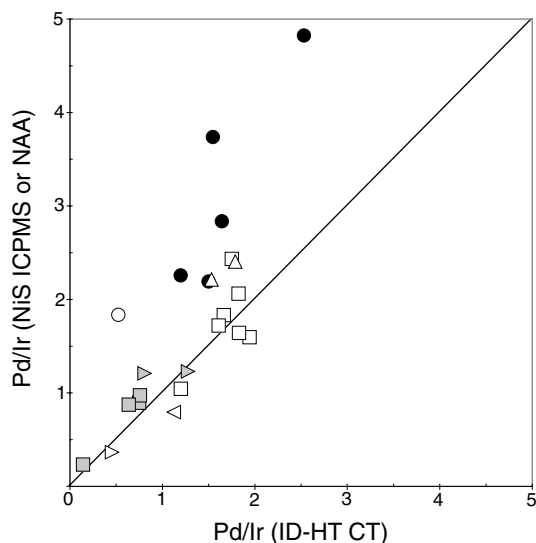
Fig. A2. Pd/Ir in samples analyzed by NiS fire assay-ICP-MS (Lorand et al., 1999, 2000), NiS fire assay-NAA (Lorand et al., 1993; Snow and Schmidt, 1998) and radiochemical NAA (Morgan, 1986) plotted against isotope dilution and high-temperature Carius tube digestion data (this work). Symbols as in Fig. 2.
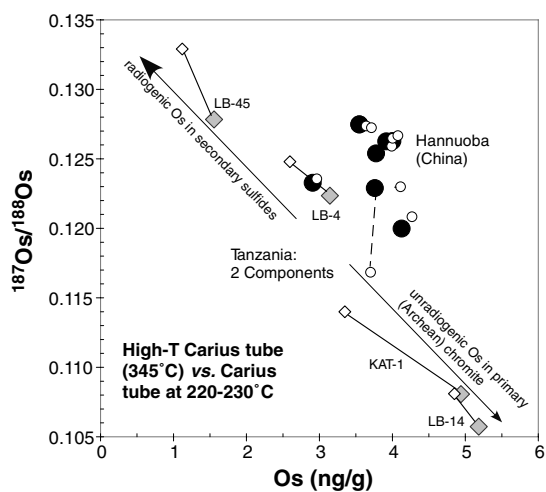

Fig. A3. $^{187}Os/^{188}Os$–Os diagram. Peridotites from Tanzania (diamonds) and Hannuoba, China (circles) were analyzed by isotope dilution and high-temperature Carius tube digestion at 345 °C (this work, large symbols) and at 220–230 °C (small symbols, this work, Chesley et al., 1999; Gao et al., 2002). Tie lines connect same sample aliquots showing large differences using different techniques. Data on samples from Tanzania indicates the presence of an easily accessible radiogenic component, presumably residing in secondary sulfides along grain boundaries, and an unradiogenic Archean component, presumably residing in phases that are difficult to digest (Os–Ru–Ir alloys, chromite) and only accessed when digested at high temperatures.

be somewhat more refractory than Ir. Pd/Ir and other ratios involving Pt-group HSE in the numerator and Ir-group HSE in the denominator tend to be overestimated in fire assay digestion because of incomplete extraction of refractory Ir-group PGE relative to Pt-group PGE. It should be noted that the high Pd/Ir (and Pt/Ir) for the

Lorand et al. (1993) data on lherzolites from Lanzo (Fig. A2) reflect too high Pd and Pt concentrations rather than low Ir (Table 3 and Lorand et al., 2000).

Fig. A3 shows a comparison of Os concentration and isotopic data obtained by isotope dilution and high-temperature Carius tube digestion at 345 °C and data obtained on the same samples by Carius tube digestion at 220–230 °C. For lherzolites from Hannuoba (China) agreement between both techniques is good, except for one sample that may be isotopically heterogeneous. Data for samples from Tanzania show substantial isotopic and concentration differences between aliquots processed under different conditions. Samples digested at 345 °C (Table 3) all show higher Os concentrations and less radiogenic $^{187}Os/^{188}Os$ compared to digestions at 220–230 °C (Chesley et al., 1999). The least radiogenic composition (LB-14) indicates an Archean age of melt extraction and is similar to that found in residual chromites from these xenoliths. Because these chromites also have high Os abundances, the systematic differences in Fig. A3 suggest incomplete digestion of chromites or Ir-group alloy inclusions in the digestions at lower temperature. Fig. A3 also shows that a component with suprachondritic $^{187}Os/^{188}Os$ and low Os concentration is present in all four samples, presumably residing in secondary sulfides along grain boundaries and reflecting silicate melt addition (Chesley et al., 1999). Another interesting feature of the new data on Labait samples are the systematically higher Re concentrations of the low-temperature digestions, which cannot be explained by incomplete digestion. These may reflect heterogeneities in the relatively coarse sample powders, which have been reground before the high-temperature digestions. We note that similar discrepancies in Re abundances appear for samples for which only limited material was available (most of the UM samples).

References

Alard, O., Griffin, W.L., Lorand, J.P., Jackson, S.E., O'Reilly, S.J., 2000. Non-chondritic distribution of the highly siderophile elements in mantle sulfides. *Nature* **407**, 891–894.

Alard, O., Griffin, W.L., Pearson, N.J., Lorand, J.-P., O'Reilly, S.Y., 2002. New insights into the Re–Os systematics of sub-continental lithospheric mantle from in situ analysis of sulfides. *Earth Planet. Sci. Lett.* **203**, 651–663.

Anbar, A.D., Zahnle, K.J., Arnold, G.L., Mojzsis, S.J., 2001. Extraterrestrial iridium, sediment accumulation and the habitability of the early Earth's surface. *J. Geophys. Res. Solid Earth* **106**, 3219–3236.

Ballhaus, C., Ellis, D.J., 1996. Mobility of core melts during Earth's accretion. *Earth Planet. Sci. Lett.* **143**, 137–145.

Becker, H., 1996. Geochemistry of garnet peridotite massifs from lower Austria and the composition of deep lithosphere beneath a Paleozoic convergent plate margin. *Chem. Geol.* **134**, 49–65.

Becker, H., Morgan, J.W., Walker, R.J., MacPherson, G.J., Grossman, J.N., 2001a. Rhenium–osmium systematics of calcium–aluminium-rich inclusions in carbonaceous chondrites. *Geochim. Cosmochim. Acta* **65**, 3379–3390.

Becker, H., Shirey, S.B., Carlson, R.W., 2001b. Effects of melt percolation on the Re–Os systematics from a Paleozoic convergent plate margin. *Earth Planet. Sci. Lett.* **188**, 107–121.

Bockrath, C., Ballhaus, C., Holzheid, A., 2004. Fractionation of the platinum-group elements during mantle melting. *Science* **305**, 1951–1953.

Bodinier, J.-L., Dupuy, C., Dostal, J., 1988. Geochemistry and petrogenesis of eastern Pyrenean peridotites. *Geochim. Cosmochim. Acta* **52**, 2893–2907.

Bodinier, J.-L., Godard, M., 2003. Orogenic, ophiolitic and abyssal peridotites. In: Holland, H.D., Turekian, K.K. (Eds.), *Treatise on Geochemistry*, vol. 2. Elsevier.

Bodinier, J.L., 1988. Geochemistry and petrogenesis of the Lanzo peridotite body, western Alps. *Tectonophysics* **149**, 67–88.

Bodinier, J.L., Menzies, M.A., Thirlwall, M.F., 1991. Continental to oceanic mantle transition-REE and Sr–Nd isotopic geochemistry of the Lanzo massif. *J. Petrol. Spec. Lherzolite Issue*, 191–210.

Brandon, A.D., Norman, M.D., Walker, R.J., Morgan, J.W., 1999. ^{186}Os–^{187}Os Systematics of Hawaiian Picrites. *Earth Planet. Sci. Lett.* **172**, 25–42.

Brandon, A.D., Snow, J.E., Walker, R.J., Morgan, J.W., 2000. ^{190}Pt–^{186}Os and ^{187}Re–^{187}Os systematics of abyssal peridotites. *Earth Planet. Sci. Lett.* **177**, 319–335.

Brandon, A.D., Walker, R.J., Puchtel, I.S., Becker, H., Humayun, M., Revillon, S., 2003. 186Os–187Os systematics of Gorgona Island komatiites: implications for early growth of the inner core. *Earth Planet. Sci. Lett.* **206**, 411–426.

Brügmann, G.E., Arndt, N.T., Hofmann, A.W., Tobschall, H.J., 1987. Noble metal abundances in komatiite suites from Alexo, Ontario, and Gorgona Island, Columbia. *Geochim. Cosmochim. Acta* **51**, 2159–2169.

Büchl, A., Brügmann, G., Batanova, V.G., Münker, C., Hofmann, A.W., 2002. Melt percolation monitored by Os isotopes and HSE abundances: a case study from the mantle section of the Troodos Ophiolite. *Earth Planet. Sci. Lett.* **204**, 385–402.

Burton, K.W., Schiano, P., Birck, J.-L., Allegre, C.J., 1999. Osmium isotope disequilibrium between mantle minerals in a spinel–lherzolite. *Earth Planet. Sci. Lett.* **172**, 311–322.

Chabot, N.L., Campbell, A.J., Jones, J.H., Humayun, M., Lauer Jr., H.V., 2006. The influence of carbon on trace element partitioning behavior. *Geochim. Cosmochim. Acta* **70**, 1322–1335.

Chen, J.H., Papanastassiou, D.A., Wasserburg, G.J., 1998. Re–Os systematics in chondrites and the fractionation of the platinum group elements in the early solar system. *Geochim. Cosmochim. Acta* **62**, 3379–3392.

Chesley, J.T., Rudnick, R.L., Lee, C.-T., 1999. Re–Os systematics of mantle xenoliths from the East African Rift: age, structure, and history of the Tanzanian craton. *Geochim. Cosmochim. Acta* **63**, 1203–1217.

Chou, C.-L., 1978. Fractionation of siderophile elements in the earth's upper mantle. In: Proceedings of the Lunar and Planetary Science Conference 9th, 219–230.

Chyba, C.F., 1991. Terrestrial mantle siderophiles and the lunar impact record. *Icarus* **92**, 217–233.

Drake, M.J., 2000. Accretion and primary differentiation of the Earth: a personal journey. *Geochim. Cosmochim. Acta* **64**, 2363–2370.

Elthon, D., 1992. Chemical trends in abyssal peridotites: refertilization of depleted suboceanic mantle. *J. Geophys. Res.* **97**, 9015–9025.

Ertel, W., O'Neill, H.S.C., Sylvester, P.J., Dingwell, D.B., Spettel, B., 2001. The solubility of rhenium in silicate melts: Implications for the geochemical properties of rhenium at high temperatures. *Geochim. Cosmochim. Acta* **65**, 2161–2170.

Frost, D.J., Liebske, C., Langenhorst, F., McCammon, C.A., Tronnes, R.G., Rubie, D.C., 2004. Experimental evidence for the existence of iron-rich metal in the Earth's lower mantle. *Nature* **428**, 409–412.

Gao, S., Rudnick, R.L., Carlson, R.W., McDonough, W.F., Liu, Y.-S., 2002. Re–Os evidence for replacement of ancient mantle lithosphere beneath the North China craton. *Earth Planet. Sci. Lett.* **198**, 307–322.

Gros, M., Lorand, J.-P., Luguet, A., 2002. Analysis of platinum group elements and gold in geological materials using NiS fire assay and Te coprecipitation; the NiS dissolution step revisited. *Chem. Geol.* **185**, 179–190.

Handler, M.R., Bennett, V.C., 1999. Behavior of platinum-group elements in the subcontinental mantle of eastern Australia during variable metasomatism and melt depletion. *Geochim. Cosmochim. Acta* **63**, 3597–3618.

Hart, S.R., Zindler, A., 1986. In search of a bulk-earth composition. *Chem. Geol.* **57**, 247–267.

Hartmann, W.K., Ryder, G., Dones, L., Grinspoon, D., 2000. The time-dependent intense bombardment of the primordial Earth/Moon system. In: Canup, R.M., Righter, K. (Eds.), *Origin of the Earth and Moon*. University of Arizona Press, pp. 493–512.

Hertogen, J., Janssens, M.-J., Takahashi, H., Palme, H., Anders, E., 1977. Lunar basins and craters: evidence for systematic compositional changes of bombarding population. In: Proceedings of Lunar and Planetary Science Conference, 17–45.

Hoashi, M., Brooks, R.R., Reeves, R.D., 1993. Palladium, platinum and ruthenium in iron meteorites and their taxonomic significance. *Chem. Geol.* **106**, 207–218.

Hofmann, A.W., 1997. Mantle geochemistry: the message from oceanic volcanism. *Nature* **385**, 219–229.

Holzheid, A., Sylvester, P., O'Neill, H.S.C., Rubie, D.C., Palme, H., 2000. Evidence for a late chondritic veneer in the Earth's mantle from high-pressure partitioning of palladium and platinum. *Nature* **406**, 396–399.

Horan, M.F., Walker, R.J., Morgan, J.W., Grossman, J.N., Rubin, A.E., 2003. Highly siderophile elements in chondrites. *Chem. Geol.* **196**, 5–20.

Jagoutz, E., Palme, H., Baddenhausen, H., Blum, K., Cendales, M., Dreibus, G., Spettel, B., Lorenz, V., Wanke, H., 1979. The abundances of major, minor and trace elements in the Earth's mantle as derived from primitive ultramafic nodules. In: Proceedings of the Lunar and Planetary Science Conference 10th, 2031–2050.

James, O. B., 1995. Siderophile elements in lunar impact melts define nature of the impactors. In: Proceedings of Lunar and Planetary Science Conference, 603–604.

Jones, J., Drake, M., 1986. Core formation and Earth's late accretionary history. *Nature* **323**, 470.

Jones, J.H., Malvin, D.J., 1990. A nonmetal interaction model for the segregation of trace element metals during solidification of Fe–Ni–S, Fe–Ni–P, and Fe–Ni–S–P alloys. *Metallurg. Trans.* **21B**, 697–706.

Kramers, J.D., 1998. Reconciling siderophile element data in the Earth and Moon, W isotopes and the upper lunar age limit in a simple model of homogenous accretion. *Chem. Geol.* **145**, 461–478.

Lee, C.-T., Rudnick, R.L., 1999. Compositionally stratified cratonic lithosphere: petrology and geochemistry of peridotite xenoliths from the Labait Volcano, Tanzania. In: Proceedings of the International Kimberlite Conference 7th, 503–521.

Lorand, J.-P., Alard, O., 2001. Platinum-group element abundances in the upper mantle: new constraints from in situ and whole-rock analyses of Massif Central xenoliths (France). *Geochim. Cosmochim. Acta* **65**, 2789–2806.

Lorand, J.-P., Pattou, L., Gros, M., 1999. Fractionation of platinum-group elements and gold in the upper mantle: a detailed study in pyrenean orogenic lherzolites. *J. Petrol.* **40**, 957–981.

Lorand, J.-P., Schmidt, G., Palme, H., Kratz, K.-L., 2000. Highly siderophile element geochemistry of the Earth's mantle: new data for the Lanzo (Italy) and Ronda (Spain) orogenic peridotite bodies. *Lithos* **53**, 149–164.

Lorand, J.P., Keays, R.R., Bodinier, J.L., 1993. Copper and noble metal enrichment across the lithosphere-asthenosphere boundary of mantle diapirs: evidence from the Lanzo lherzolite massif. *J. Petrol.* **34**, 1111–1140.

Luguet, A., Lorand, J.P., Seyler, M., 2003. A coupled study of sulfide petrology and highly siderophile element geochemistry in abyssal peridotites from the Kane Fracture Zone (MARK area, Mid-Atlantic ridge). *Geochim. Cosmochim. Acta* **67**, 1553–1570.

McDonough, W.F., Sun, S.-s., 1995. The composition of the Earth. *Chem. Geol.* **120**, 223–253.

Meibom, A., Sleep, N.H., Chamberlain, C.P., Colemen, R.G., Frei, R., Hren, M.T., Wooden, J.L., 2002. Re–Os isotopic evidence for long-

lived heterogeneity and equilibration processes in the Earth's upper mantle. *Nature* **419**, 705–708.

Meisel, T., Fellner, N., Moser, J., 2003a. A simple procedure for the determination of platinum group elements and rhenium (Ru, Rh, Pd, Re, Os, Ir, and Pt) using ID-ICP-MS with an inexpensive on-line matrix separation in geological and environmental materials. *J. Anal. Atomic Spectr.* **18**, 720–726.

Meisel, T., Moser, J., 2004. Reference materials for geochemical PGE analysis: new analytical data for Ru, Rh, Pd, Os, Ir, Pt and Re by isotope dilution ICP-MS in 11 geological reference materials. *Chem. Geol.* **208**, 319–338.

Meisel, T., Reisberg, L., Moser, J., Carignan, J., Melcher, F., Brügmann, G., 2003b. Re–Os systematics of UB–N, a serpentinized peridotite reference material. *Chem. Geol.* **201**, 161–179.

Meisel, T., Walker, R.J., Irving, A.J., Lorand, J.-P., 2001. Osmium isotopic compositions of mantle xenoliths: a global perspective. *Geochim. Cosmochim. Acta* **65**, 1311–1323.

Minarik, W.G., Ryerson, F.J., Watson, E.B., 1996. Textural entrapment of core-forming melts. *Science* **272**, 530–533.

Morgan, J.W., 1986. Ultramafic xenoliths: clues to Earth's late accretionary history. *J. Geophys. Res.* **91** (B12), 12,375–12,387.

Morgan, J.W., Horan, M.F., Walker, R.J., Grossman, J.N., 1995. Rhenium–osmium concentration and isotope systematics in group IIAB iron meteorites. *Geochim. Cosmochim. Acta* **59**, 2331–2344.

Morgan, J.W., Walker, R.J., Brandon, A.D., Horan, M.F., 2001. Siderophile elements in the Earth's upper mantle and lunar breccias: data synthesis suggests manifestations of the same late influx. *Meteorit. Planet. Sci.* **36**, 1257–1275.

Murthy, V.-R., 1991. Early differentiation of the Earth and the problem of mantle siderophile elements: a new approach. *Science* **253**, 303–306.

Norman, M.D., Bennett, V.C., Ryder, G., 2002. Targeting the impactors: siderophile element signatures of lunar impact melts from Serenitatis. *Earth Planet. Sci. Lett.* **2002**, 217–228.

O'Neill, H.S.C., 1991. The origin of the Moon and the early history of the Earth: a chemical model. Part 2: the Earth. *Geochim. Cosmochim. Acta* **55**, 1159–1172.

Palme, H., Nickel, K.G., 1985. Ca/Al ratio and composition of the earth's upper mantle. *Geochim. Cosmochim. Acta* **49**, 2123–2132.

Parkinson, I.J., Hawkesworth, C.J., Cohen, A.S., 1998. Ancient mantle in a modern arc: osmium isotopes in Izu-Bonin-Mariana forearc peridotites. *Science* **281**, 2011–2013.

Pattou, L., Lorand, J.P., Gros, M., 1996. Non-chondritic platinum-group element ratios in the Earth's upper mantle. *Nature* **379**, 712–715.

Pearson, D.G., Canil, D., Shirey, S.B., 2003. Mantle samples included in volcanic rocks: xenoliths and diamonds. In: Holland, H.D., Turekian, K.K. (Eds.), *Treatise on Geochemistry*, vol. 2. Elsevier, pp. 171–275.

Pearson, D.G., Irvine, G.J., Ionov, D.A., Boyd, F.R., Dreibus, G.E., 2004. Re–Os isotope systematics and platinum group element fractionation during mantle melt extraction: a study of massif and xenolith peridotite suites. *Chem. Geol.* **208**, 29–59.

Pernicka, E., Wasson, J.T., 1987. Ru, Re, Os, Pt and Au in iron meteorites. *Geochim. Cosmochim. Acta* **51** (6), 1717–1726.

Peters, T., Stettler, A., 1987. Time, physico-chemical conditions, mode of emplacement and geologic setting of the Totalp peridotite in the eastern Swiss Alps. *Schweiz. Mineral. Petrogr. Mitt.* **67**, 285–294.

Puchtel, I.S., Humayun, M., 2005. Highly siderophile element geochemistry of 187Os-enriched 2.8 Ga Kostomuksha komatiites, Baltic Shield. *Geochim. Cosmochim. Acta* **69**, 1607–1618.

Puchtel, I.S., Humayun, M., Campbell, A.J., Sproule, R.A., Lesher, C.M., 2004. Platinum group element geochemistry of komatiites from the Alexo and Pyke Hill areas, Ontario, Canada. *Geochim. Cosmochim. Acta* **68**, 1361–1383.

Rehkämper, M., Halliday, A.N., Alt, J., Fitton, J.G., Zipfel, J., Takazawa, E., 1999a. Non-chondritic platinum-group element ratios in abyssal peridotites: petrogenetic signature of melt percolation? *Earth Planet. Sci. Lett.* **172**, 65–81.

Rehkämper, M., Halliday, A.N., Barfod, D., Fitton, G.J., Dawson, J.B., 1997. Platinum-group element abundance patterns in different mantle environments. *Science* **278**, 1595–1598.

Rehkämper, M., Halliday, A.N., Fitton, J.G., Lee, D.C., Wieneke, M., Arndt, N.T., 1999b. Ir, Ru, Pt and Pd in basalts and komatiites: new constraints for the geochemical behavior of the platinum group elements in the mantle. *Geochim. Cosmochim. Acta* **63**, 3915–3934.

Reisberg, L., Lorand, J.-P., 1995. Longevity of sub-continental mantle lithosphere from osmium isotope systematics in orogenic peridotite massifs. *Nature* **376**, 159–162.

Reisberg, L., Zhi, X., Lorand, J.P., Wagner, C., Peng, Z., Zimmermann, C., 2005. Re–Os and S systematics of spinel peridotite xenoliths from east central China: evidence for contrasting effects of melt percolation. *Earth Planet. Sci. Lett.* **239**, 286–308.

Reisberg, L.C., Allegre, C.J., Luck, J.-M., 1991. The Re–Os systematics of the Ronda ultramafic complex of southern Spain. *Earth Planet. Sci. Lett.* **105**, 196–213.

Righter, K., Drake, M.J., 1997. Metal-silicate equilibrium in a homogeneously accreting Earth: new results for Re. *Earth Planet. Sci. Lett.* **146**, 541–553.

Righter, K., Walker, R.J., Warren, P.H., 2000. Significance of highly siderophile elements and Os isotopes in the lunar and terrestrial mantles. In: Canup, R., Righter, K. (Eds.), *Origin of the Earth and Moon*. University of Arizona Press, pp. 291–322.

Ringwood, A.E., 1979. *Origin of the Earth and Moon*. Springer-Verlag.

Rudnick, R.L., Gao, S., Ling, W.-L., Liu, Y.-S., McDonough, W.F., 2004. Petrology and geochemistry of spinel peridotite xenoliths from Hannuoba and Qixia, North China craton. *Lithos* **77**, 609–637.

Rushmer, T., Minarik, W.G., Taylor, G.J., 2000. Physical processes of core formation. In: Canup, R., Righter, K. (Eds.), *Origin of the Earth and Moon*. University of arizona Press, pp. 227–243.

Ryder, G., Koeberl, C., Mojzsis, S.J., 2000. Heavy bombardment of the Earth at ∼ 3.85 Ga: the search for petrographic and geochemical evidence. In: Canup, R.M., Righter, K. (Eds.), *Origin of the Earth and Moon*. University of Arizona Press, pp. 475–492.

Saal, A.E., Takazawa, E., Frey, F.A., Shimizu, N., Hart, S.R., 2001. Re–Os isotopes in the horoman peridotite: evidence for refertilization. *J. Petrol.* **42**, 25–37.

Schmidt, G., 2004. Are high-temperature fractionations in the solar nebula preserved in highly siderophile element systematics of the Earth's mantle? *Meteorit. Planet. Sci.* **39**, 1995–2007.

Schmidt, G., Snow, J.S., 2002. Os isotopes in mantle xenoliths from the Eifel volcanic field and the Vogelsberg (Germany): age constraints on the lithospheric mantle. *Contrib. Mineral. Petrol.* **143**, 694–705.

Schmidt, G., Palme, H., Kratz, K.-L., Kurat, G., 2000. Are highly siderophile elements (PGE, Re and Au) fractionated in the upper mantle. New results on peridotites from Zarbargad. *Chem. Geol.* **163**, 167–188.

Shen, J.J., Papanastassiou, D.A., Wasserburg, G.J., 1996. Precise Re–Os determinations and systematics of iron meteorites. *Geochim. Cosmochim. Acta* **60**, 2887–2900.

Shirey, S.B., Walker, R.J., 1995. Carius tube digestions for low-blank rhenium–osmium analysis. *Anal. Chem.* **67**, 2136–2141.

Smoliar, M.I., Walker, R.J., Morgan, J.W., 1996. Re–Os ages of group IIA, IIIA, IVA, and IVB iron meteorites. *Science* **271**, 1099–1102.

Snow, J.E., Dick, H.J.B., 1995. Pervasive magnesium loss by marine weathering of peridotite. *Geochim. Cosmochim. Acta* **59** (20), 4219–4235.

Snow, J.E., Schmidt, G., 1998. Constraints on Earth accretion deduced from noble metals in the oceanic mantle. *Nature*, 166–169.

Staudigel, H., Plank, T., White, B., Schmincke, H.-U., 1996. Geochemical fluxes during seafloor alteration of the basaltic upper oceanic crust: DSDP sites 417 and 418. In: Bebout, G. (Ed.), *Subduction: Top to Bottom*, Vol. 96. American Geophysical Union, pp. 19–38.

Sun, S.-S., 1982. Chemical composition and origin of the Earth's primitive mantle. *Geochim. Cosmochim. Acta* **46**, 179–192.

Tackley, P.J., 2000. Mantle convection and plate tectonics: toward an integrated physical and chemical theory. *Science* **288**, 2003–2007.

Tagle, R., 2005. LL-Ordinary chondrite impact on the Moon: results from the 3.9 Ga impact melt at the landing site of Apollo 17. Lunar and Planetary Science Conference, Abstract #.

Walker, D., 2000. Core participation in mantle geochemistry: geochemical Society Ingerson Lecture, GSA Denver, October 1999. Geochim. Cosmochim. Acta 64, 2897–2911.

Walker, R.J., Brandon, A.D., Bird, J.M., Piccoli, P.M., McDonough, W.F., Ash, R.D., 2005. ^{187}Os–^{186}Os systematics of Os–Ir–Ru alloy grains from southwestern Oregon. *Earth Planet. Sci. Lett.* **230**, 211–226.

Walker, R.J., Horan, M.F., Morgan, J.W., Becker, H., Grossman, J.N., 2002. Comparative 187Re–187Os systematics of chondrites: implications regarding early solar system processes. *Geochim. Cosmochim. Acta* **66**, 4187–4201.

Walker, R.J., Horan, m.F., Shearer, C.K., Papike, J.J., 2004. Low abundances of highly siderophile elements in the lunar mantle: evidence for prolonged late accretion. *Earth Planet. Sci. Lett.* **224**, 399–413.

Walker, R.J., Morgan, J.W., Smoliar, M.I., Beary, E., Czamanske, G.K., Horan, M.F., 1997. Applications of the 190Pt–186Os isotope system to geochemistry and cosmochemistry. *Geochim. Cosmochim. Acta* **61**, 4799–4808.

Wasson, J.T., 1999. Trapped melt in IIIAB irons; solid/liquid elemental partitioning during the fractionation of the IIIAB magma. *Geochim. Cosmochim. Acta* **63**, 2875–2889.

Wolf, R., Woodrow, A., Anders, E., 1979. Lunar basalts and pristine highland rocks: comparison of siderophile and volatile elements, 2107–2130.

Zindler, A., Hart, S.R., 1986. Chemical geodynamics. *Annu. Rev. Earth Planet. Sci.* **14**, 493–571.